Title

Relative Toxicity of Exhaust Particulate After Accelerated Thermal Oxidation of Recycled Vegetable Oil Biodiesel Fuel

Authors

Russo, Joseph
Holmén, Britt A.

Publication Date

2024-11-01

DOI

10.7922/G2RF5SCZ

Data Availability

The data associated with this publication are within the manuscript.

Relative Toxicity of Exhaust Particulate After Accelerated Thermal Oxidation of Recycled Vegetable Oil Biodiesel Fuel

November 2024

A Research Report from the National Center for Sustainable Transportation

Joseph Russo, University of Vermont

Britt A. Holmén, University of Vermont

National Center for Sustainable Transportation
A USDOT University Transportation Center

THE UNIVERSITY OF VERMONT
TRANSPORTATION RESEARCH CENTER

TECHNICAL REPORT DOCUMENTATION PAGE

1. Report No. NCST-UVM-RR-24-22	**2. Government Accession No.** N/A	**3. Recipient's Catalog No.** N/A
4. Title and Subtitle Relative Toxicity of Exhaust Particulate After Accelerated Thermal Oxidation of Recycled Vegetable Oil Biodiesel Fuel		**5. Report Date** November 2024 **6. Performing Organization Code** N/A
7. Author(s) Joseph Russo Britt A. Holmén, PhD, https://orcid.org/0000-0003-3020-4293		**8. Performing Organization Report No.** N/A
9. Performing Organization Name and Address University of Vermont Transportation Research Center Mansfield House 25 Colchester Avenue, Burlington, VT 05405		**10. Work Unit No.** N/A **11. Contract or Grant No.** USDOT Grant 69A3551747114
12. Sponsoring Agency Name and Address U.S. Department of Transportation Office of the Assistant Secretary for Research and Technology 1200 New Jersey Avenue, SE, Washington, DC 20590		**13. Type of Report and Period Covered** Final Report (September 2018 – December 2019) **14. Sponsoring Agency Code** USDOT OST-R

15. Supplementary Notes
DOI: https://doi.org/10.7922/G2RF5SCZ

16. Abstract
Given that today's real-world diesel fuel supply is comprised of biodiesel as a blendstock with petrodiesel, understanding how addition of biodiesel affects exhaust particle properties and their subsequent effect on human health is critically important. Here, samples of a commercial waste vegetable oil biodiesel B100 fuel were subject to thermal oxidation at 110°C for 5, 10 or 20 hr before diesel engine dynamometer emissions testing as the neat fuel (B100) and as a 20% v/v biodiesel blend (B20) with petrodiesel. Exhaust particulate matter samples collected using impingers were tested for the ability of the particles to initiate formation of reactive oxygen species (ROS) using the abiotic dithiothreitol (DTT) assay. DTT Activity [nmol DTT consumed per minute per mg PM] of three B20, three B100 as well as petrodiesel (B0) fuels over a total of 13 emissions tests with a light-duty diesel engine were compared. Combining data for emissions tests by fuel blend and oxidation status, mean DTT Activity was similar between B0 and B20 (10hr oxidized), B100 (neat) and B100 (5 hr). Particles from the B20 neat and B20 (20 hr) fuels had the highest measured DTT Activity whereas the B100 neat and B100 (5 hr) had the lowest DTT Activity. Twenty hours of thermal oxidation conditions resulted in the highest measured DTT Activity (or highest potential to form ROS) for both B20 and B100 fuels and IP=0. An inverse relationship between storage stability (opposite of degree of fuel oxidation) of the biodiesel fuel as measured by induction potential (IP) and the ROS formation potential: higher DTT Activity was noted for the B100 fuels with the lowest IP. Results suggest that mixing of B20 from certified B100 fuel may lead to oxidation of unsaturated FAMES and subsequent higher ROS formation potential. Future work should examine how the detailed chemical composition of biodiesel exhaust PM, especially when waste oil B100 is blended with petrodiesel at 20 % v/v, may be related to DTT consumption or other metrics for ROS formation potential. Further, future emissions studies should provide information on property differences between Bxx blends and the neat B100 fuel that result not only from biodiesel storage, but from fuel handling.

17. Key Words Biodiesel, dithiothreitol (DTT), ROS, B20, B100, oxidative stability, FAMEs		**18. Distribution Statement** No restrictions.	
19. Security Classif. (of this report) Unclassified	**20. Security Classif. (of this page)** Unclassified	**21. No. of Pages** 70	**22. Price** N/A

Form DOT F 1700.7 (8-72) Reproduction of completed page authorized

NCST

About the National Center for Sustainable Transportation

The National Center for Sustainable Transportation is a consortium of leading universities committed to advancing an environmentally sustainable transportation system through cutting-edge research, direct policy engagement, and education of our future leaders. Consortium members include: the University of California, Davis; California State University, Long Beach; Georgia Institute of Technology; Texas Southern University; the University of California, Riverside; the University of Southern California; and the University of Vermont. More information can be found at: ncst.ucdavis.edu.

Disclaimer

The contents of this report reflect the views of the authors, who are responsible for the facts and the accuracy of the information presented herein. This document is disseminated in the interest of information exchange. The report is funded, partially or entirely, by a grant from the U.S. Department of Transportation's University Transportation Centers Program. However, the U.S. Government assumes no liability for the contents or use thereof.

The U.S. Department of Transportation requires that all University Transportation Center reports be published publicly. To fulfill this requirement, the National Center for Sustainable Transportation publishes reports on the University of California open access publication repository, eScholarship. The author may copyright any books, publications, or other copyrightable materials developed in the course of, or under, or as a result of the funding grant; however, the U.S. Department of Transportation reserves a royalty-free, nonexclusive and irrevocable license to reproduce, publish, or otherwise use and to authorize others to use the work for government purposes.

Acknowledgments

This study was funded, partially or entirely, by a grant from the National Center for Sustainable Transportation (NCST), supported by the U.S. Department of Transportation (USDOT) through the University Transportation Centers program. The author would like to thank the NCST and the USDOT for their support of university-based research in transportation, and especially for the funding provided in support of this project. Laboratory work contributed by Jack Reed and Markus Ingelsson are especially noted.

NCST

Relative Toxicity of Exhaust Particulate After Accelerated Thermal Oxidation of Recycled Vegetable Oil Biodiesel Fuel

A National Center for Sustainable Transportation Research Report

November 2024

Joseph Russo, Transportation Research Center, University of Vermont

Britt A. Holmén, Civil & Environmental Engineering, University of Vermont

NCST

[page intentionally left blank]

TABLE OF CONTENTS

1.0 Introduction: Background on Biodiesel Fuel, Tailpipe Emissions, and PM Health Effects 1
1.1 Biodiesel and U.S. Energy Policy 1
1.2 Biodiesel Composition 2
1.3 Biodiesel Storage Stability 3
1.4 Exhaust Particles from Vehicles 5
1.5 Waste Grease Biodiesel as a Sustainable Fuel 5
1.6 Study Objectives 6
1.7 Chemical Assay for Reactive Oxygen Species (ROS) Formation Potential 7
2.0 Methods 7
2.1 Fuel Sources, Blending and Diesel Engine Testing 7
2.2 Accelerated Thermal Oxidation of B100 fuel & Measured Fuel Oxidation Level 9
2.3 Measuring Particle Oxidation Potential (DTT Assay) 10
2.4 GCMS Analysis of FAMEs in Biodiesel Fuel Blends 12
3.0 Results and Discussion 14
3.1 DTT Assay Results – Neat and Oxidized Biodiesel Fuel PM 14
3.2 Fuel Composition – FAMEs 18
3.3 B100 Induction Period Effects on DTT Activity 21
3.4 DTT Assay Sanity Check: “PM Activity” Results WMBD vs UCONN Samples 24
5.0 Conclusions 26
References 27
Appendix A. Drop Method Standard Operating Procedure 31
Appendix B. Impinger Data 46
1.0 DTT Assay – Raw Data 46
1.1 Comparison to Prior DTT Assay Work in TAQ Lab 49
1.2 Intrasample Variability in DTT Assay Data 49
Appendix C. Gas Chromatography – Mass Spectrometry Information 51
1.0 Calibration Curves for Individual FAMEs using SIM Analysis 53

List of Tables

Table 1. DTT assay impingers and engine tests by fuel blend and oxidation level/time. 11
Table 2. Ten Fatty Acid Methyl Esters (FAMEs) in Nu-Chek Prep Standard GLC 124. 13
Table 3. Comparison of neat and aged biodiesel fuel blends: DTT activity magnitude. 18
Table C1. GCMS quantitation method (scan mode). 52
Table C2. Unsaturated FAME concentrations relative to NEAT fuel (OX = 0). 52
Table C3. GCMS calibration curve best-fit slopes for SIM Acquisition. 58
Table C4. DTT activity (nmol DTT/min/mg PM). 58

List of Figures

Figure 1. U.S. production volumes of biodiesel (circles) and renewable diesel (triangles) compared to the renewable fuel standard (RFS) annual targets for “biomass-based diesel” (dashed line). Data from USDA Bioenergy Statistics and US EPA. 2

Figure 2. (a) Base-catalyzed transesterification to produce biodiesel. (b) Structures of common C18:x FAMEs in biodiesel. 4

Figure 3. Unsaturated FAMES in waste vegetable oil (WVO) biodiesel exhaust PM [29]. 6

Figure 4. Pyramid Drive Cycle (PDC), a symmetrical stepped modal drive cycle that varied engine load between 10% and 50%. 8

Figure 5. Example particle number distribution in Armfield light-duty diesel engine exhaust collected by Scanning Mobility Particle Sizer during Mode 3 of the PDC emissions test cycle (see Figure 4) for six test runs on different fuels (B0 and B100 only). 9

Figure 6. DTT Activity (nanomol DTT consumed per minute per milligram of PM) for individual duplicate DTT Assays for each impinger. 15

Figure 7. Mean DTT Activity (nmol DTT/min/milligram PM) for each impinger; x-axis labels also show the fuel blend code. 16

Figure 8. Mean DTT Activity (nmol DTT/min/milligram PM) by biodiesel fuel / accelerated oxidation time blend. 17

Figure 9. Saturated FAME concentrations in B20 [left] and B100 [right] fuels as a function of oxidation time (hrs). 19

Figure 10. Unsaturated FAME concentrations in B20 [left] and B100 [right] fuels as a function of oxidation time (hrs). 20

Figure 11. Relative concentration of unsaturated FAMEs in B20 [Left] and B100 [Right] fuels that experienced accelerated oxidation conditions compared to the respective neat fuel. 20

Figure 12. The three phases of oxidation for polyunsaturated FAMEs after Christensen and McCormick (2014) [16]. 23

Figure 13. Results for White Mountain Biodiesel (WMBD) Fuel B100 sample induction period (*x*-axis) and DTT Activity (*y*-axis) based on exhaust PM impinger samples after fuel combustion in a light-duty diesel engine. 24

Figure 14. Two ratios of unsaturated FAMEs for fuels studied here (B20 and B100) and in prior work with UCONN biodiesel blends (B10, B20, B50 and B100) of soybean (SOY) and waste vegetable oil (WVO) feedstock biodiesel. 25

Figure A1. Key supplies. A: Small cylinder. B: Millipore Forceps. C: Foil lined Petri dish top. D: Foil lined Petri dish, bottom. E: Large cylinder. 32

Figure A2. How to hold impinger sample on vortexer. 32

Figure A3. Desiccator (F) with desiccant (G). 33

Figure A4. Coy Chamber (left)with Cahn Microbalance (right). 33
Figure A5. 100 uL Drummond Micro Pipetter (top) and tip (bottom) with ruler for scale. 33
Figure A6. Ultra-pure Nitrogen tank (Right) and Nitrogen blowdown station (Left). 34
Figure A7. The ETS control box associated with the humidity conditions in the Coy Chamber... 34
Figure A8. Dickson logger..... 34
Figure A9. Aluminum foil cup top view (top) and side view (bottom) with ruler for scale. 36
Figure A10. An example photo of Mettler Toledo XPE26. 42
Figure B1. Normalized DTT assay experimental time points (TP1 to 100) for each PM impinger, Assay Blank and PQN quality control sample. 46
Figure B2. Raw data normalized to TP1=26.235 uM DTT, the theoretical value initially in each cuvet at start of the DTT assay. 47
Figure B3. DTT Activity (nmol DTT/min/microgram PM) for individual duplicate DTT Assays for each impinger labelled by the fuel blend (Excel chart). 48
Figure B4. DTT Activity for PM impinger samples from two exhaust emissions studies with the same VW engine, but different driving cycles and biodiesel fuel sources. 49
Figure B5. [Left] Individual impinger DTT Activity (nmol DTT/min/mgPM) results, organized by blend with color of circle indicating oxidation time (0=none, 5, 10 or 20 hr). [Right] Same data, but symbol shows mean +/- 1 SD of the duplicate DTT Assay measurements for each impinger. 50
Figure B6. One-way analysis of variance test results for impinger sample DTT Activity by hours of B100 fuel oxidation. 50
Figure C1. GCMS Selected Ion Monitoring (SIM) acquisition parameters. 51
Figure C2. Calibration curve for C22:0 FAME, methyl behenate. 53
Figure C3. Calibration curve for C18:3 FAME, methyl linolenate. 53
Figure C4. Calibration curve for C20:0 FAME, methyl arachidate. 54
Figure C5. Calibration curve for C18:2cis FAME, methyl linoleate. 54
Figure C6. Calibration curve for C18:2trans FAME, methyl linoelaidate. 55
Figure C7. Calibration curve for C18:1cis FAME, methyl oleate. 55
Figure C8. Calibration curve for C18:1trans FAME, methyl elaidate. 56
Figure C9. Calibration curve for C18:0 FAME, methyl stearate. 56
Figure C10. Calibration curve for C16:0 FAME, methyl palmitate. 57
Figure C11. Calibration curve for C14:0 FAME, methyl myristate. 57
Figure C12. Mean concentrations (ng/uL) of individual FAMEs in B20 and B100 fuel. 59

Figure C13. Unsaturated FAME concentrations (ng/uL) in B20 and B100 fuels. 59
Figure C14. Induction Potentials measured by BOSS for WMBD B100 fuels of 0, 5, 10, 20 hrs of accelerated oxidation. 60

Relative Toxicity of Exhaust Particulate After Accelerated Thermal Oxidation of Recycled Vegetable Oil Biodiesel Fuel

1.0 Introduction: Background on Biodiesel Fuel, Tailpipe Emissions, and PM Health Effects

1.1 Biodiesel and U.S. Energy Policy

Since 2005, U.S. energy policy has mandated increased renewable fuels use for transportation, including "biomass-based diesel" or biodiesel. Biodiesel, a mixture of long-chain (16 to 18 carbons) fatty acid methyl esters (FAMEs), is derived from a variety of animal or vegetable oil feedstocks and is a preferred alternative to petroleum diesel because it: (i) offers air pollution benefits; (ii) can be blended into existing petroleum diesel fuel supplies with no engine modifications; (iii) is an important strategy for both domestic energy independence and sustainable agricultural production; and (iv) reduces net greenhouse gas emissions compared to petrodiesel [1].

In the United States, biofuel production and use are generally the incentivized results of federal and state policies that include the EPA's Renewable Fuel Standard (RFS) and California's Low Carbon Fuel Standard (LCFS). Since 2005, the RFS set annual domestic biofuel production targets that grew from 0.5 billion gallons in 2009 to 1.70-1.90 billion gallons in 2015-2017 [2, 3]. However, the original RFS "by 2022" target of 36 billion gallons of 'total renewable fuels' was achieved chiefly with corn ethanol, a fuel with questionable greenhouse gas lifecycle metrics compared to biodiesel. Initial biodiesel production volumes did increase rapidly under the RFS in response to RFS tax credits, but in January 2023 biodiesel production was for the first time exceeded by a new "biomass-based diesel" fuel, "renewable diesel" (Figure 1). Renewable diesel (RD) is produced in refineries using the same feedstocks as biodiesel but is produced using a more energy- and capital-intensive 'hydrotreating' production process that results in a final fuel composition similar to petroleum diesel: 100% hydrocarbons, with no oxygen (unlike FAME biodiesel). RD similarly benefits from the biodiesel tax credit which Congress intended to offset the higher production cost of these alternative fuels relative to petrodiesel. The historic zig-zag pattern of biodiesel production in Figure 1 tracks with the availability of these annual tax credits; recently the Inflation Reduction Act of 2022 extended this credit through 2024 (EIA 2023) [4].

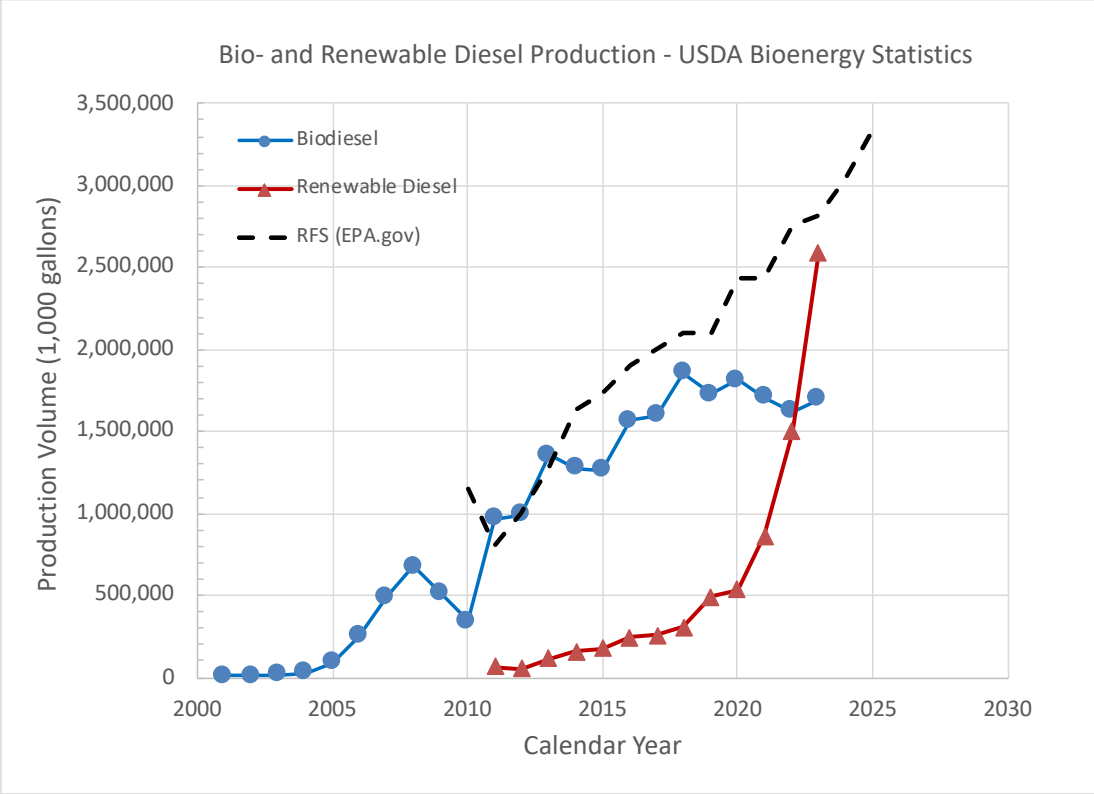

Figure 1. U.S. production volumes of biodiesel (circles) and renewable diesel (triangles) compared to the renewable fuel standard (RFS) annual targets for "biomass-based diesel" (dashed line). Data from USDA Bioenergy Statistics and US EPA.

1.2 Biodiesel Composition

Transesterification converts the triglycerides in biodiesel feedstock materials—animal fats, virgin and recycled plant and animal waste oils—to a mixture of C_{16}-C_{22} fatty acid methyl esters (FAMEs) that meets federal standards for on-road biodiesel fuel (e.g., ASTM D6751) [5]. Neat biodiesel is nearly free of sulfur and aromatic compounds, can be blended with petroleum diesel and is readily used in on-road vehicles in up to a 20% biodiesel blend (B20, 20% bio- and 80% petro-diesel, by volume), chiefly of soybean oil feedstock in the USA. Lower blend ratios (5 or 10%) are often used in winter climates to protect against fuel gel formation due to biodiesel's higher cloud point [6, 7]. Different plant/animal fats naturally contain various proportions of saturated and unsaturated FAMEs that affect fuel combustion and tailpipe emissions. Use of waste cooking oil feedstocks instead of virgin plant oils may result in biodiesel with elevated transition metal concentrations that are 2 to 8 times higher than petrodiesel (some metals—Cu, Fe and Zn—are high because of leaching from cooking utensils) [8, 9]. Transition metals are of interest because Fenton-type reactions (Eq. 1) form the biologically-reactive hydroxyl radical, •OH:

$$Fe^{2+} + HOOH \rightarrow Fe^{3+} + {}^{\bullet}OH + OH^{-} \qquad [1]$$

Compared to petrodiesel, neat biodiesel fuel has approximately an 11% higher oxygen content. These oxygen molecules reduce the biofuel's energy density and alter the products of combustion. Prior work shows both higher and lower exhaust concentrations of potentially toxic oxygenated organic combustion products such as aldehydes, ketones and carboxylic acids [10, 11, 12, 13], suggesting combustion conditions (i.e., engine operating mode) as well as biodiesel fuel feedstock and fuel storage conditions may affect exhaust composition. Very little research has been done to evaluate how biodiesel fuel oxidation during storage affects the resulting exhaust toxicity. Here, the focus is on exhaust particulate matter (PM).

Given the generally strong association between the adverse health effects of airborne particulate matter, especially fine particulate matter ($PM_{2.5}$; aerodynamic diameter $\leq$ 2.5 micrometers), and oxidative stress derived from reactive oxygen species (ROS[1]) formation in living cells, it is important to fully characterize the "toxicity" of biodiesel exhaust particles in terms of their ability to generate ROS. Here, an abiotic chemical assay is employed to examine the degree to which PM in exhaust from a diesel engine fueled using 'aged' biodiesel from waste oil feedstock increases ROS formation compared to the neat (i.e., unoxidized) fuel.

1.3 Biodiesel Storage Stability

Renewable, carbon-neutral, biomass-based fuels such as biodiesel could be part of the solution to the global sustainable energy challenge of the 21st century if critical decisions regarding the optimal biofuel feedstocks are based on data that weigh competing energy, environmental, and public health effects associated with the fuel's production, transport and use. Biodiesel use as a transportation fuel has advantages such as reducing fossil fuel dependency, lowering greenhouse gas (GHG) and some criteria air pollutant emissions, and improving the lubricity of ultralow sulfur diesel fuel (ULSD[2]). However, a challenge arises in relating biodiesel fuel composition to combustion emissions and subsequent environmental and health effects: namely biodiesel's tendency to oxidize during storage.

Biodiesel is considerably less stable to atmospheric oxidation than traditional petrodiesel fuel because biodiesel is comprised of mono- and poly-unsaturated long-chain fatty acid methyl esters (FAMEs). The composition of the original feedstock oils/grease used to manufacture biodiesel fuel via base-catalyzed transesterification (Figure 2) affects the fuel's susceptibility to deterioration during fuel storage and use. Typically, the fatty acid chains in biodiesel feedstock fats and oils have 16 to 18 carbons and up to three double bonds separated by single methylene carbons that prevent conjugation. Common names (and number of double bonds) for the unsaturated 18-carbon chain fatty acids are oleic (c18:1), linoleic (c18:2) and linolenic (c18:3; see Figure 2). The non-conjugated carbon-carbon double bonds in unsaturated FAME aliphatic chains are susceptible to attack by atmospheric oxygen. The rate of FAME oxidation depends on biodiesel fuel storage conditions (temperature, light, fuel additives, metals,

[1] Reactive oxygen species (ROS) include hydroxyl, hydroperoxyl, and organic peroxyl radicals as well as hydrogen peroxide, superoxide anion and organic peroxides.

[2] Petrodiesel de-sulfurization lowers the fuel's lubricity compared to high sulfur petrodiesel (see Farahani 2009) (14).

humidity, free fatty acids) as well as the chemical composition (i.e., mixture of FAMEs: structure and number of methylene-interrupted C=C double bonds) of the biodiesel feedstock [15]. Oxidation of these unsaturated FAMEs during fuel storage (or during fuel recycling in the diesel engine fuel system) changes the composition of biodiesel fuel to first form hydroperoxides ("primary oxidation products") and ultimately shorter-chain secondary oxidation products such as carboxylic acids, ketones, and aldehydes [16]. FAMEs oxidation can proceed further to produce polymeric sediments that compromise the fuel's basic properties and may adversely affect engine performance.

The oxygen-bearing organic oxidation products in the biodiesel fuel are known to have associated adverse human health effects, but unknown effects on fuel performance (combustion) and resulting exhaust composition. In practice, to prevent oxidative deterioration of the fuel, biodiesel manufacturers include antioxidant additives in their fuel formulations. Little is known about the functional lifetimes of these antioxidants under real-world fuel storage and in-vehicle use. Long-term fuel storage may produce partially or even fully oxidized biodiesel fuel that is then used in diesel engines. The timescale for diesel fuel recirculation to consume the fuel's antioxidants is also unknown. **This study was conceived to examine the hypothesis that oxidation of biodiesel fuel will result in measurable changes in the exhaust particulate from the diesel engine tailpipe that could have adverse effects on human health.**

a. $$Triglyceride + 3\ CH_3OH + NaOH\ (cat.) \rightarrow \quad Fatty\ Ester\ Mixture + Glycerin + H_2O\ \ldots.\{side\ products: free\ fatty\ acids, Na^+, diglyceride\ \}$$

b.

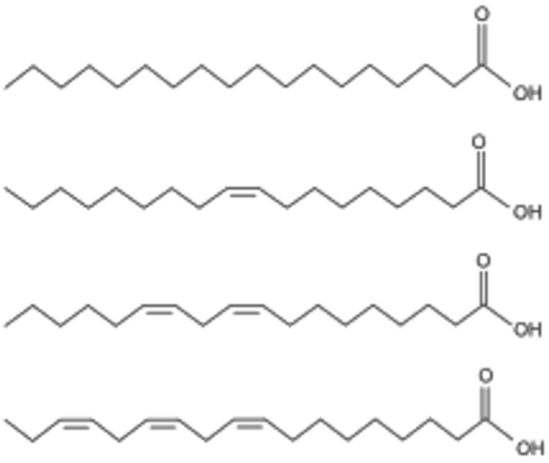

Stearic	18:0
Oleic	18:1
Linoleic	18:2
Linolenic	18:3

Figure 2. (a) Base-catalyzed transesterification to produce biodiesel. (b) Structures of common C18:x FAMEs in biodiesel. For example, the most highly unsaturated FAME in biodiesel is linolenic acid methyl ester, or methyl linolenate, C18:3, $C_{19}H_{32}O_2$, due to the three C-C double bonds in its fatty acid chain.

1.4 Exhaust Particles from Vehicles

Because extensive evidence associates airborne particles with adverse human health effects [17-26] and the continued importance of vehicle exhaust contributions to nanoscale (diameter < 100nm) particle emissions, it is critical that we understand and quantify possible interventions that mitigate human exposure to these potentially toxic airborne particles. Numerous studies to date have compared petrodiesel to biodiesel exhaust emissions, but with varying results on which fuel is "better" in terms of tailpipe emissions. Comparison across different studies is difficult because of the variation in test methods, fuel type (including biofuel preparation and additives), engine operating cycles and the chosen outcome metrics between laboratories. It is rare for research studies to measure and report on biodiesel fuel composition due to the expense of full fuel chemical characterization. Instead, fuel properties are the only fuel data reported, if any fuel information is provided at all. Further, studies generally do not report on biodiesel fuel additives or storage conditions (time, temperature, container etc.) prior to emissions testing. One variable possibly overlooked by many researchers conducting biodiesel emissions studies is the fact that biodiesel fuel is more chemically reactive than petrodiesel. In other words, biodiesel sitting around the laboratory may "age" due to the fuel's sensitivity to atmospheric oxidation. There is a second mechanism by which biodiesel fuel may be oxidized prior to engine combustion. Unlike gasoline-powered vehicles, diesel vehicles continually recirculate fuel between the engine and the fuel tank [15]. Excess fuel (above that necessary to achieve combustion for the demanded power output) is continually drawn from the fuel tank to lubricate and cool the engine's high pressure fuel system. This excess fuel is heated by the engine, but then returns to the fuel tank, carrying the rejected heat. Although no studies can be found on chemical changes in fuel composition during diesel engine operation, it is reasonable to expect some alteration of fuel properties during these repeated fuel circulation cycles due to the high temperatures involved in vehicle engines combined with headspace in the fuel tank. Thus, there are four possible ways to "age" (oxidize) biodiesel and its blends [27]: (1) during fuel storage (B100 and Bxx blends); (2) fuel handling to create Bxx blends; (3) recirculation in diesel fuel tank during vehicle operation (Bxx); and (4) via high temperatures in vehicle's engine/fuel system (Bxx).

1.5 Waste Grease Biodiesel as a Sustainable Fuel

In the US, soybeans are the primary biodiesel feedstock, but also an important food source. *Recycled* cooking waste vegetable oils and animal grease are alternative biodiesel fuel feedstocks that help divert the more than 3 billion gallons of waste grease generated annually in the US away from wastewater treatment plants or animal feed rendering facilities [28]. Many municipalities currently use waste grease biodiesel fuel in vehicles as well as for residential heating. Use of recycled waste oil/grease eliminates the "food vs fuel" controversy that arose in the early days of biodiesel production (~2008) in the US because using soybeans as the primary virgin biodiesel fuel feedstock diverted soybean critical crops for human and animal food.

1.6 Study Objectives

Very little is known about the differential health effects of petrodiesel vs biodiesel combustion particles. Even less is known about the relative toxicity of combusted oxidized biodiesel fuel and the tendency of recycled waste vegetable oil B100 to improve or aggravate the health effects associated with diesel engine exhaust. This research quantifies the extent to which oxidized biodiesel fuel has an increased tendency to create exhaust particles that have a higher potential to form reactive oxygen species (ROS) compared to petroleum diesel combustion particles. We report results from an abiotic chemical assay to compare the relative tendency of diesel engine exhaust particulate matter (PM) to form ROS. Formation of reactive oxygen species on particle surfaces is associated with inducing oxidative stress in cells and therefore the chemical assay is a relative metric of combustion particle toxicity. Most available information on biodiesel oxidation discusses the fuel's oxidation stability in storage, a required fuel property for commercial fuel sale. There is relatively little information on changes in chemical composition due to fuel oxidation and how these changes relate to the toxicity of subsequent exhaust emissions when the fuel is combusted.

Our previous work quantified the fatty acid methyl esters (FAMEs) in un-oxidized biodiesel fuel blends and combustion particles using traditional gas chromatography- mass spectrometry methods, Kasumba and Holmén 2016 [29]. The emission rates of mono- and poly-unsaturated FAMEs increased with the proportion of biodiesel in the fuel blend (Figure 3), as one would expect.

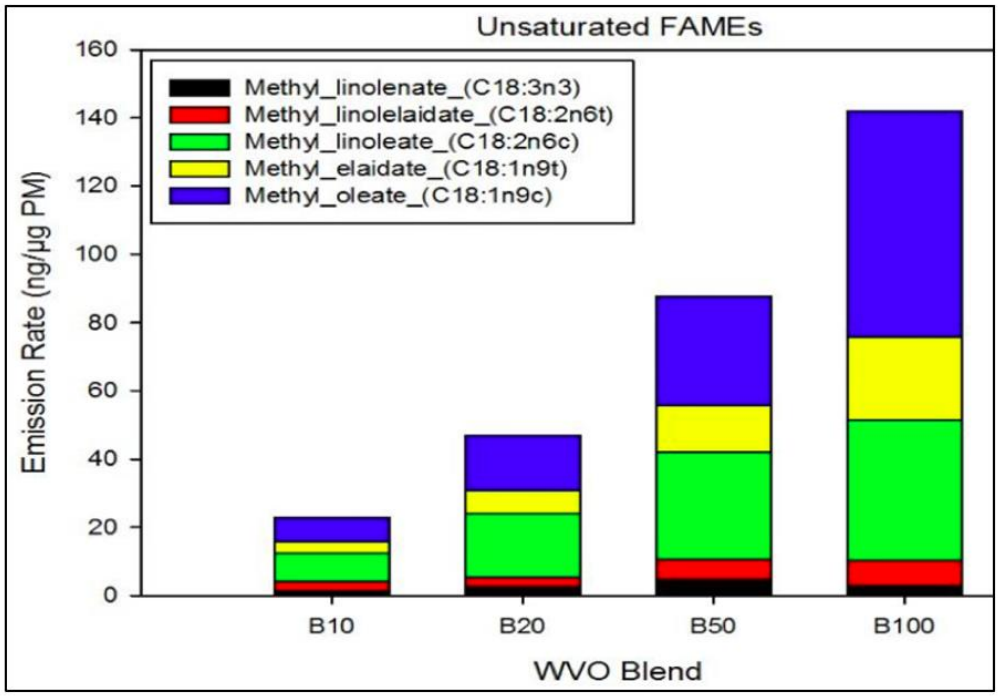

Figure 3. Unsaturated FAMES in waste vegetable oil (WVO) biodiesel exhaust PM [29].

1.7 Chemical Assay for Reactive Oxygen Species (ROS) Formation Potential

Adverse human health effects of nanoparticles from both petro- and biodiesel combustion products in vehicle exhaust are thought to involve oxidative stress at the cellular level, either indirectly by particles contributing to reactive oxygen species (ROS) production, or directly via ROS-bearing functionalities within the particles. Thus, a number of studies have quantified the "oxidative potential" of exhaust particles using a chemical assay with dithiothreitol (DTT) [30, 31] or other cell-free assays [32-38]. The water soluble organic carbon fraction of biodiesel PM has been associated with particle oxidative potential and ROS formation has been shown to increase with higher percentages of biodiesel in the fuel blend [34, 36, 39]. In this study, a modified version of the Charrier and Anastasio (2012) [31] DTT assay is used to evaluate the "toxicity" of exhaust particles derived from combustion of different biodiesel fuels in a light-duty diesel engine running a laboratory modal emissions test cycle.

In summary, while the FAME composition of biodiesel has often been related to fuel performance and regulated primary emissions, to our knowledge, *no prior studies have evaluated the toxicity of neat and aged biodiesel fuel particle emissions and the relationships to fuel composition and stability.*

2.0 Methods

2.1 Fuel Sources, Blending and Diesel Engine Testing

Biodiesel-free petroleum diesel was sourced from a local gas station (Maplefields, South Burlington, VT) and either used directly or blended with a commercial B100 biodiesel (White Mountain Biodiesel, North Haverhill, NH) to make a v/v B20 blend via splash blending with inversion mixing. The White Mountain Biodiesel B100 feedstock is used cooking oils. All biodiesel fuel blends were prepared and stored in 5 gal HDPE buckets with tight-fitting lids and nitrogen gas replaced air in the bucket headspace during fuel storage.

Emissions tests were conducted on the various fuel types—B0 (petrodiesel), B20 and B100—in an Armfield CM-12 light-duty diesel Volkswagen engine dynamometer on a computer-controlled 9-mode stepped symmetrical drive cycle (Figure 4). Particulate matter (PM) in the engine exhaust was collected over the full 9-mode emissions test using Teflon impingers containing 30 mL of ethanol. PM concentrations in the impinger samples was measured using our "Drop Method" wherein 100uL aliquots of the impinger suspensions were dried in a desiccator to evaporate the ethanol and the PM mass was determined using a Cahn C-33 microbalance with 1 microgram sensitivity (see Drop Method details in Appendix A). In addition to collecting PM in impingers, PM was collected on Teflon filters and real-time instruments were used to measure exhaust gases (5-Gas Analyzer; CO, CO_2, NOx, O_2 and HC) and particle number (Scanning mobility particle sizer, SMPS, TSI, Inc., long DMA and ultrafine CPC).

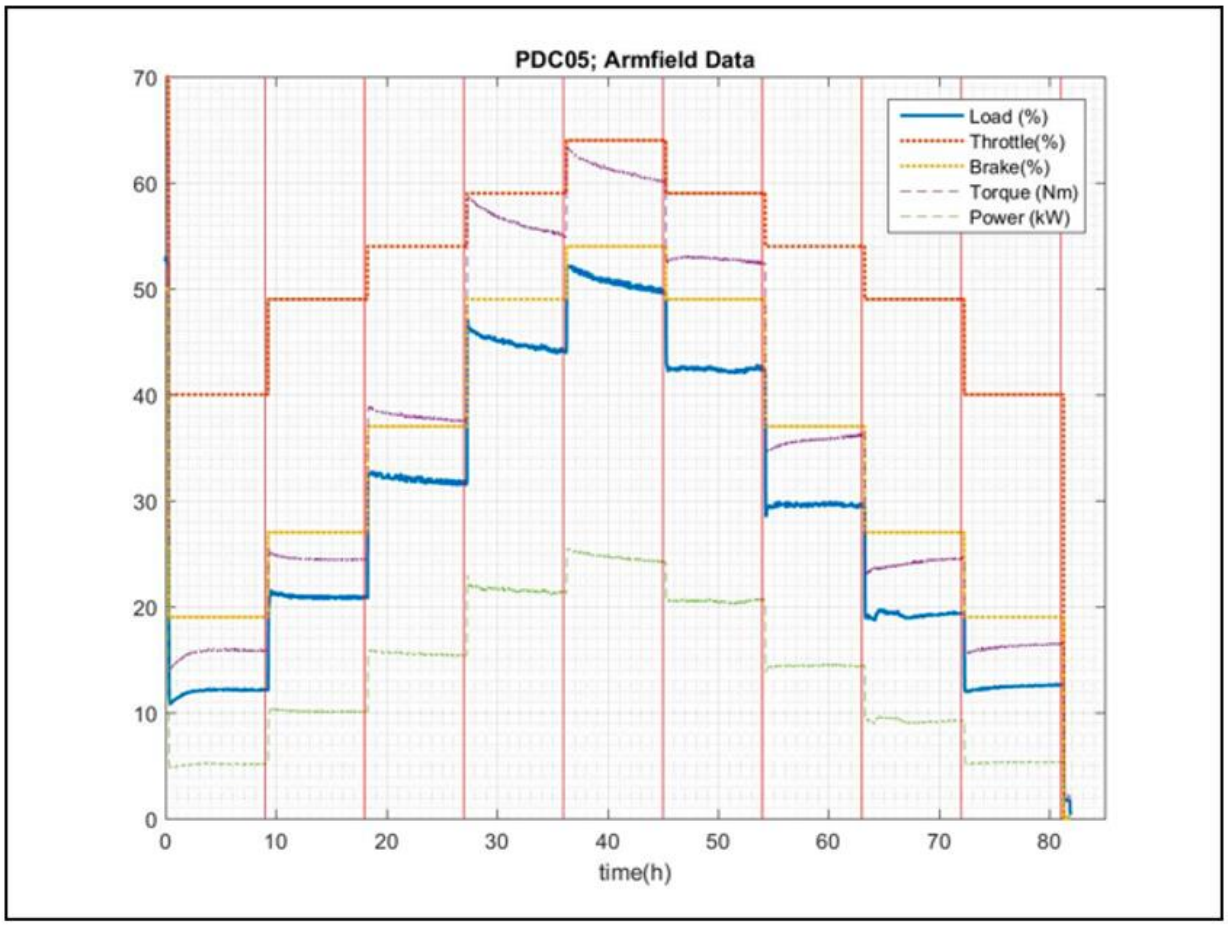

Figure 4. Pyramid Drive Cycle (PDC), a symmetrical stepped modal drive cycle that varied engine load between 10% and 50%. The load was increased in 5 steps and then decreased in 4 steps over the approximately 80-minute emissions test time. The engine load (%), engine throttle (%), dynamometer brake (%), engine torque (N-m) and engine power (kW) recorded by the Armfield dynamometer were generally consistent over each mode of the drive cycle.

Particle exhaust emissions typically vary somewhat between individual emissions tests on the same fuel. Figure 5 shows the variability was chiefly observed in absolute particle concentration for a given biodiesel or petrodiesel (B0) fuel not the size range of ultrafine particles emitted. For example, the two largest peaks (solid lines, Figure 5) were from a different petrodiesel company (Trono fuels, Burlington VT) than used to prepare the White Mountain Biodiesel/ Maplefield petrodiesel B20 biodiesel blend (dashed lines, Figure 5) evaluated in this study.

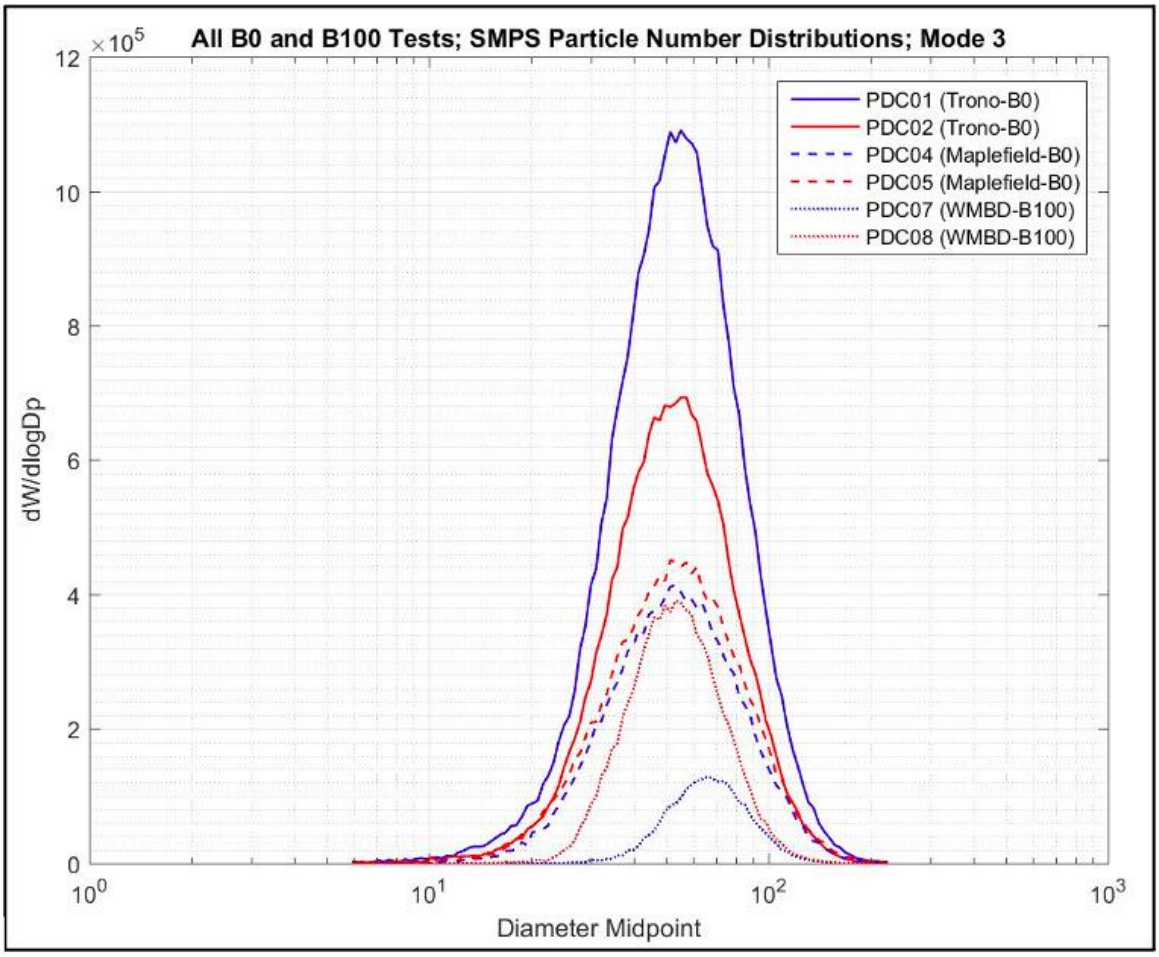

Figure 5. Example particle number distribution in Armfield light-duty diesel engine exhaust collected by Scanning Mobility Particle Sizer during Mode 3 of the PDC emissions test cycle (see Figure 4) for six test runs on different fuels (B0 and B100 only). WMBD = White Mountain Biodiesel.

2.2 Accelerated Thermal Oxidation of B100 fuel & Measured Fuel Oxidation Level

Details on the procedures used to "age" the neat B100 fuel are described in Jack Reed's master's thesis (Reed 2021) [40] and only briefly reviewed here for completeness. Portions of the as-received B100 fuel from White Mountain Biodiesel LLC (North Haverhill, NH) was thermally oxidized in 4-L glass vessels on a laboratory hotplate at 110°C for 5, 10 and 20 hr durations in a hood with constant "vortex" stirring. The Biodiesel Oxidation Stability Surveyor (BOSS) was custom-built by Jack Reed and Markus Ingelsson to measure biodiesel fuel induction period (IP) following specifications in method EN15751. [41] Induction period is measured in hours and B100 fuels must exceed IP = 3 hr for commercial sale at the fuel pump. BOSS instrument accuracy and repeatability were verified by testing a set of four B100 neat biodiesel fuel samples generously donated by Iowa Central Fuels Testing Laboratory after testing at their

facility using a commercial Rancimat device (the instrument specified in regulation EN15751). Relative standard deviation on replicate measures with the BOSS were less than 22% and accuracy, measured as percent difference between BOSS and Iowa-reported Rancimat data, ranged from 8-50%, with BOSS values always lower than the Iowa Rancimat values. With the exception of one outlier (50%) the BOSS measures of IP were deemed acceptable for relative comparisons across the aged B100 biodiesel fuels. The average IP for quadruplicate measurements (n=4) on the BOSS for the White Mountain Biodiesel (WMBD) waste vegetable oil B100 fuel was 6.03 hours, with a 1.33 standard deviation and an RSD of 22.03%, meeting the requirement set in ASTM D6751 for a minimum induction period of 3.0 hours. As expected, BOSS results showed a decrease in measured induction period with increasing accelerated thermal aging time of the B100 fuel, in agreement with IP vs time trends in the literature [16, 42-44]. See Jack Reed's MS Thesis [40] for details on the accelerated oxidation protocols used in handling the B100 fuel. It should be noted that the thermal oxidation procedures were only carried out on the neat B100 fuel, not the blended B20.

2.3 Measuring Particle Oxidation Potential (DTT Assay)

The abiotic dithiothreitol (DTT) method [30, 31] was used to quantify the ability of diesel exhaust particles to generate reactive oxygen species (ROS) that are linked to the adverse health effects of ultrafine particles [45]. The more DTT consumed per mass of PM, the higher the particles' ROS formation potential [46]. The DTT Assay was carried out on 13 impingers from 2017-2018 engine testing using the Armfield CM-12 light-duty diesel engine and biodiesel fuels (B100 and B20) at various stages of accelerated oxidation (0 hr, 5 hr, 10 hr and 20 hr). As documented in Table 1, each impinger was collected from a different run of the CM-12 diesel engine using various fuel compositions (B0, B20 or B100 blends).

We adopted a modified method from Charrier & Anastasio (2012) used previously in our lab (Holmén et al. 2017) [47] that is quantitative and carried out in phosphate buffer at pH 7.3 in a constant temperature bath at 37°C. The assay requires monitoring sample composition over time after adding an initial concentration at t=0 of 186.27 uM DTT to each 8mL glass reaction vial. For quality control (QC), the redox active quinone 9,10-phenanthraquinone (PQN) was the positive control and assay blanks containing reagents and metal-free phosphate buffer served as the negative control. For each impinger sample and control, duplicate assay vials, denoted A and B, were run each analysis day. Impinger samples were prepared to target a PM concentration of 25 ug/mL in the reaction vials based on our laboratory's "Drop Method" (Holmén et al. 2017) [47] that gravimetrically determines the PM concentration in a suspension. Details on the Drop Method are found in Appendix A. The Drop Method was performed after some of the more dilute collected impinger samples were concentrated to approximately 1000 ug/mL (1 mg/mL) via Speed-Vac. At ten time points ranging from 2.5 to 48 minutes, 200 uL sample aliquots were transferred to cuvets to which some DTT Assay reagents were previously added to both quench the reaction and form a yellow compound (2-nitro-5-thiobenzoic acid, TNB) that was quantified by UV-VIS spectrophotometer at 412nm wavelength. Assay blanks were run daily, in duplicate, with each set of samples as negative control and a 0.1 uM solution of phenanthrenequinone (PQN) was run daily as the positive control to check reagent viability.

A calibration curve for the DTT Assay was carried out with DTT standards prepared in cuvets using a 400 uM stock DTT solution and metal-free phosphate buffer solution at concentrations ranging from 0 to 45 uM DTT. For the PM impinger samples, 40 uL of a 0.01 M DTT Stock solution was added to each reaction vial. All DTT assay measurements for exhaust PM and the daily positive and negative controls were carried out in the dark using a red light and duplicate results were averaged. As indicated in Table 1, 13 impinger samples from 13 different emissions tests were analyzed for ROS formation potential with the DTT Assay.

Table 1. DTT assay impingers and engine tests by fuel blend and oxidation level/time.

	B0	**B20**				**B100**			
	neat	**neat**	**OX3**	**OX2**	**OX1**	**neat**	**OX3**	**OX2**	**OX1**
	0 hr	**0 hr**	**5 hr**	**10 hr**	**20 hr**	**0 hr**	**5 hr**	**10 hr**	**20 hr**
Impinger No:									
	617	619	N/A	636	623	608	631	N/A	627
	639				624	610	632		629
						635			
PDC Engine Test IDs:									
	10-1	12-1	--	21-2	14-1	07-1	18-1	--	16-1
	22-1				15-2	08-2	19-2		17-1
						20-1			

N/A = Data Not Available

The DTT Assay raw data analysis involved the following steps:

a) Review raw absorbance data in Excel Data Analysis Workbooks and double-check data entry based on review of hardcopy logsheets.

b) Compute precision statistics on replicate vials of positive and negative controls. Target was less than 15% relative standard deviation (RSD =coefficient of variation, CV, in percent) between duplicates.

c) Compute percent DTT loss and omit from further analysis all data points with DTT consumption > 30%. This data omission only applied to the PQN controls, resulting in use of just the first 5 PQN data points (of the 10 time points collected).

d) Plot DTT remaining concentration vs. elapsed time for each vial replicate for a given QC sample and impinger sample. Omit data where intercept exceeded expected value of 26.235 uM +/- 15% (range = 22.3 to 30.17). The only data omitted by this criterion was the replicate 1 Assay Blank in Exp21-043A, where absorbances were unusually high (possibly due to vial contamination).

e) Compute *normalized* DTT concentrations (i.e., normalize the DTT concentration so first time point was equal to the theoretical starting vial concentration of 186.27 uM. This is equivalent to a cuvet concentration of 26.235 uM DTT) to enable replicate analysis for impinger data collected on different DTT Assay analysis days.

f) Export data to JMP Pro 14.2.1 to use Fit Model function for Standard Least Squares linear regression on each replicate. JMP results output was combined into a new Data Table containing the fit model parameter values, SE and p-values.

g) Export JMP linear regression results and reorganize the Fit Model output in EXCEL to columns of SLOPE and INTERCEPT; Compute the Assay Blank-corrected SLOPES for each Experimental Day using the daily Assay Blank results.

h) The blank-corrected slopes for each sample correspond to the "*DTT Consumption Rates*" by the sample in micromolar DTT per min (uM DTT/min).

i) Because of differences in the exact mass of PM added to each reaction vial, the DTT Consumption Rates were converted to "*DTT Activity*" by dividing the *DTT Consumption Rate* by the calculated concentration of PM in the original DTT Assay reaction vial, based on Drop Method data for the impingers that was collected during the DTT Assay experiment.

Equation 2 shows that the raw Drop Method data on PM concentration in the impinger sample must be converted to the final "Reaction (Rxn) Vial PM concentration" using the known microliter volumes of impinger sample (V_{imp}) as well as the total volume of the Assay Vial solution (V_{vial}). The "DTT Activity" final calculation is shown in **Equation 3**. These values, in nanomoles of DTT consumed per minute per milligram of PM, were used to compare the different fuel blends.

Drop Method:

$$Rxn\ Vial\ PM\ Conc\ \left[\frac{\mu g}{mL}\right] = \frac{V_{imp}[\mu L] \times PM\ Conc|_{imp}\ [\frac{\mu g}{mL}]}{V_{Vial}[\mu L]} \quad [2]$$

DTT Assay:

$$DTT\ Activity\ \left[\frac{nmol/min}{mg_{PM}}\right] = \frac{DTT\ Consumption\ Rate\ [\frac{\mu M}{min}]}{PM\ Conc|_{imp}\ [\frac{\mu g}{mL}]}\ x\ \frac{1000\ [\mu g]}{[mg]} \quad [3]$$

2.4 GCMS Analysis of FAMEs in Biodiesel Fuel Blends

Fuel samples collected from the CM-12 engine fuel tank were stored in the freezer immediately after emissions testing. For fuel analysis, fuel samples were diluted on a w/w basis to achieve an 80 ppm sample of fuel in dichloromethane (DCM) solvent. These samples were spiked with two saturated FAME internal standards, C15:0 and C21:0, that are not found in natural waste oils and thus would not interfere with chemical analysis. Chemical standards were purchased as specialty order, Standard GLC-124, from Nu-Chek Prep (Elysian, MN). The standard included ten saturated and unsaturated FAMEs, at equal concentrations, as shown in Table 2.

Calibration curves were prepared by initial dilution of 100.00 mg of the FAMEs standard oil into a 10 mL volumetric flask (Stock 1; 10,000 ng/uL total FAMEs) with DCM, then further diluting to a second stock solution at a total FAMEs concentration of 100 ng/uL (Stock 2). Stock 2 was used

to prepare the low concentration calibration standards at nominal concentrations of each individual FAME of 0.5, 1, 2, 4 and 6 ng/uL and Stock 1 was used to prepare the high concentration standards with individual FAME concentrations of 10, 20, 50, 90 and 120 ng/uL. Linear best-fit calibration curves were prepared assuming intercept = 0 (JMP version 17.0) based on raw GCMS response normalized to the internal standard concentration in a given sample to account for injection error. Calibration curves are shown in Appendix C based on C15:0 methyl ester relative response. Relative response factors were converted to concentrations of each FAME based on the known injected concentration of IS 1, 19.396 ng/uL. Because all fuels were prepared using identical dilution procedures, data here are shown based on GC-measured concentrations without the multiplier for the initial fuel-preparation dilution to 80ppm. This simplifies the number magnitudes.

Table 2. Ten Fatty Acid Methyl Esters (FAMEs) in Nu-Chek Prep Standard GLC 124.

Chain	Common Name	Formal Name (Methyl Ester)	Wt %	MW
C14:0	Methyl Myristate	Tetradecanoic acid	10	228.38
C16:0	Methyl Palmitate	Hexadecanoic acid	10	256.43
C18:0	Methyl Stearate	Octadecanoic acid	10	284.48
C18:1t	Methyl Elaidate	9E-Octadecenoic aci	10	296.48
C18:1c	Methyl Oleate	cis-9-Octadecenoic acid	10	282.47
C18:2t	Methyl Linoelaidate	9E,12E-octadecadienoic acid	10	294.5
C18:2c	Methyl Linoleate	cis-9,12-Octadecadienoic acid	10	280.46
C20:0	Methyl Arachidate	Eicosanoic acid	10	312.54
C18:3n3	Methyl Linolenate	cis-9,12,15-Octadecatrienoic acid	10	278.44
C22:0	Methyl Behenate	Docosanoic acid	10	340.60

An Agilent 6890N/5973 gas chromatograph/mass spectrometer (GC-MS) was used to analyze the 10 FAMEs in each fuel sample using selective ion monitoring (SIM) and Chemstation software. A highly polar SLB-IL 100 column (Supelco; 30m, 0.25mm, 0.2um) was used to separate the FAME analytes and isomers. Analytical conditions included splitless injection of 1uL samples, 99.99% helium carrier gas, 1.5 mL/min flowrate, temperatures of 240°C (injector), 230°C (detector), and an oven program of 50°C (hold 1 min), 10°/min ramp to 140°C followed by a 3°/min ramp to 160°C and a final ramp at 10°/min ramp to 220°C with 1 minute final hold. Total run time was 26.67 minutes per sample. All GC-MS instrument parameters are tabulated in Appendix C. DCM blanks and two calibration standards (one high, one low) were run between every 5 fuel samples throughout the analysis sequences. Each fuel sample was run in duplicate and mean concentrations are reported.

3.0 Results and Discussion

3.1 DTT Assay Results – Neat and Oxidized Biodiesel Fuel PM

Raw impinger time plots (i.e., Normalized DTT remaining concentration (micromolar) vs. experimental time (min)) for each Assay Blank, impinger and PQN positive control are show in Figure B1 with the best-fit line for all replicates. The observed steeper slopes for the positive control (Phenanthrenequinone, PQN) are as expected compared to the nearly flat line for the Assay Blank negative controls. Exhaust PM impinger samples show slopes between these control endpoints.

Combining the DTT Assay (DTT consumed over time) and Drop Method data (PM mass in sample) using Equations [2] and [3] to give DTT Activity (in nanomol DTT consumed per minute per milligram of PM) provides a better metric to compare the relative toxicity of the individual impinger samples because it normalizes each sample's data to the mass of exhaust PM in the assay reaction vial. Figure 6 shows the individual impinger DTT Activity results, showing the variability in the DTT assay across replicates. Figure 7 highlights that variability occurs both between duplicates for a single impinger (error bar) and between different engine emission tests on the same blend of biodiesel (bars with blend brackets). Note that "20.1" denotes a B20 fuel that was artificially oxidized for 20 hrs (longest time); "100.3" is B100 oxidized for 5 hours (shortest time) and "0" is petrodiesel, "100" is neat biodiesel. The variability in the DTT Assay can be attributed to variation in emission testing conditions, in reagent quality, correction of individual impinger sample data using daily assay blanks and variability in pipetting very small volumes of impinger samples both in the DTT Assay and in the Drop Method to determine PM concentration of impinger samples.

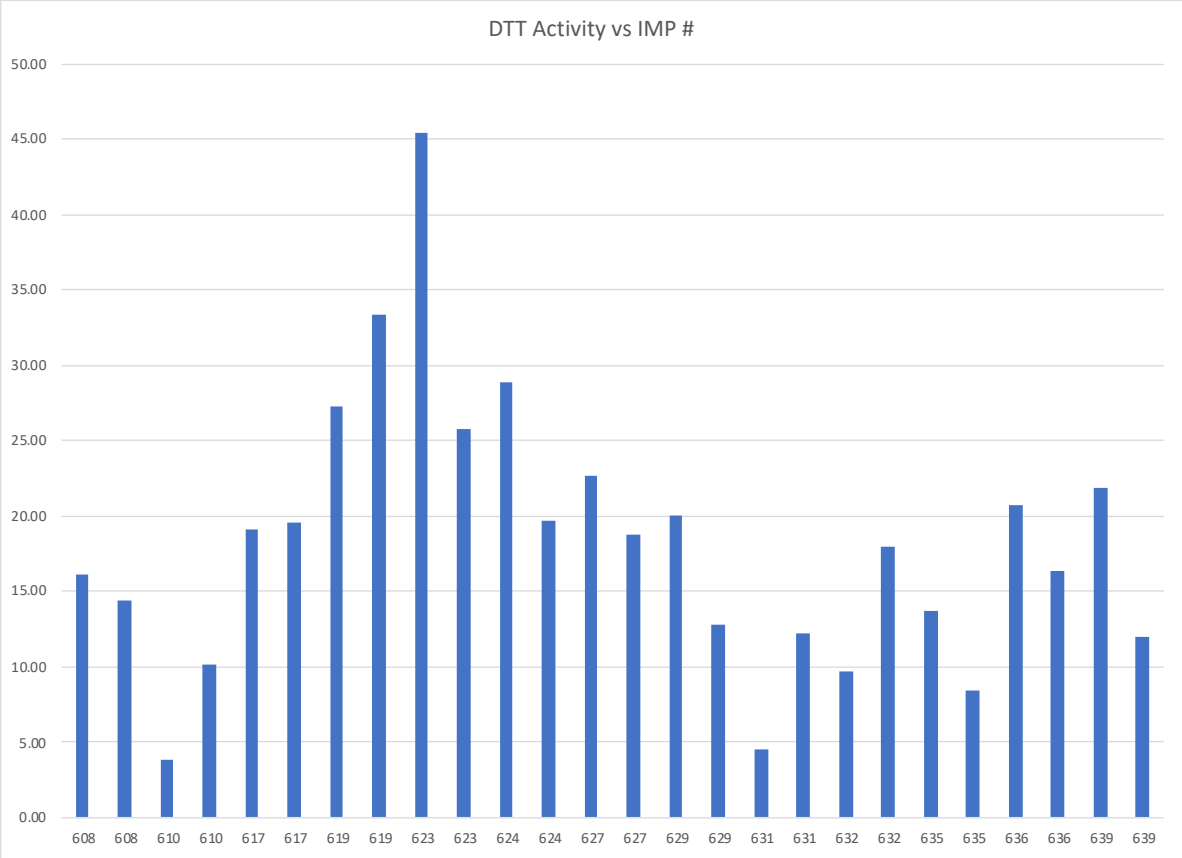

Figure 6. DTT Activity (nanomol DTT consumed per minute per milligram of PM) for individual duplicate DTT Assays for each impinger.

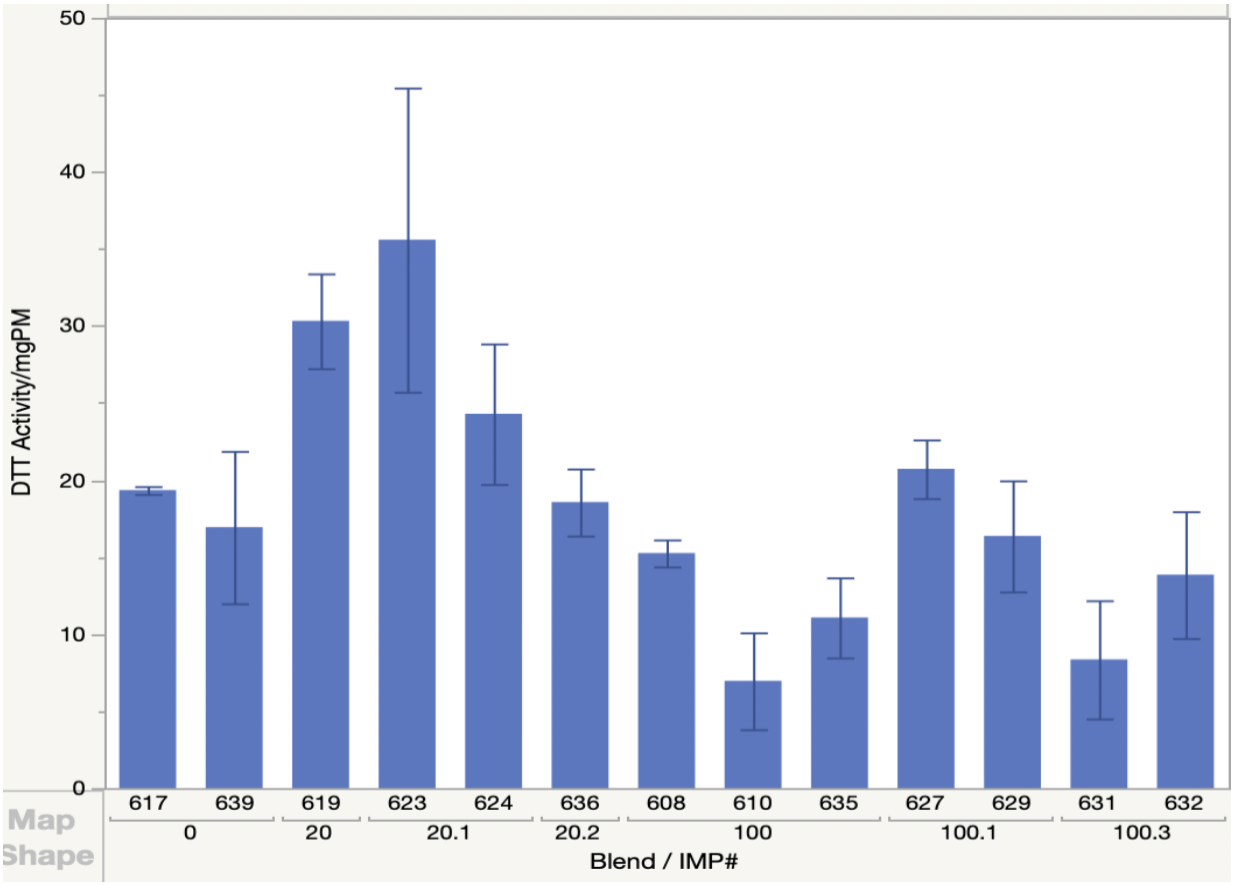

Figure 7. Mean DTT Activity (nmol DTT/min/milligram PM) for each impinger; x-axis labels also show the fuel blend code. Error bars represent one standard error (SE) between the two replicate DTT Assay tests for each impinger. Fuel blends designated as decimal number representing volume percent biodiesel and a fuel oxidation "aging" time code after the decimal point (1 = 20 hr, 2 = 10 hr, 3 = 5 hr). For example, "100.1" represents B100 fuel experienced accelerated oxidation for 20 hrs prior to emissions testing.

Combining all the replicates for each blend, Figure 8 shows higher DTT Activity for B20 blends neat and 20.1 (20 hr) compared to other fuel blends. It is observed that there does not appear to be a consistent pattern between oxidation time code (represented by the decimal – see caption) of the original B100 fuel and the DTT Activity for B20 and B100 fuels.

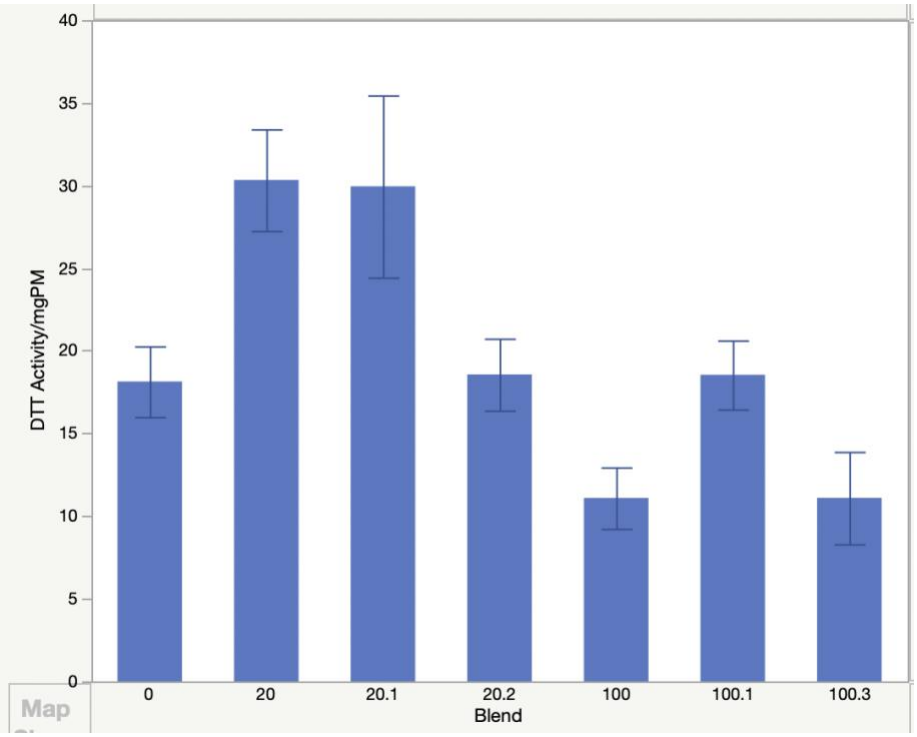

Figure 8. Mean DTT Activity (nmol DTT/min/milligram PM) by biodiesel fuel / accelerated oxidation time blend. Error bars represent one standard error (SE) among all replicates. Fuel blends designated as decimal number representing volume percent biodiesel to left of the decimal point and a fuel oxidation "aging" time code (1 = 20 hr, 2 = 10 hr, 3 = 5 hr) to right of the decimal point. For example, "100.1" represents B100 fuel that experienced accelerated oxidation for 20 hrs prior to emissions testing.

The DTT Activity with respect to accelerated aging trends is distinct for the B20 and B100 blends as described in Table 3. It should be kept in mind that the B20 fuels were prepared in the lab by splash blending a given "aged" (accelerated oxidation) B100 fuel with petrodiesel. It is possible that the various aged B20 blends experienced different levels of laboratory air exposure during handling to create the B20 blends, thus explaining some of the variability in Figure 8, including the result that neat B20 had a similar, and high, DTT Activity as 20-hr aged B20, but the 10-hr aged B20 had the lowest DTT activity across the three B20 fuels. The lack of replicate emission tests for the B20 fuels (neat and 10-hr aging; see Figure 7) may also have contributed to the irregular trend with fuel aging.

Figure 8 suggests that B100 fuel is more desirable than B0 in terms of ROS formation potential (i.e., B100 generally had lower DTT activity than B0). However, use of B100 fuel is impractical both due to lack of fuel availability and engine performance difficulties with B100 in cold weather (fuel 'gels' and clogs fuel filters). In contrast to B100, the more practical and widely available B20 blend showed the highest DTT Activity values measured in the study with means for neat B20 nearly identical to the 20-hr oxidized B20 test results. As stated above, the low number of B20 emissions tests and possibility of differences in unanticipated fuel oxidation during splash blending complicate interpretation with respect to accelerated oxidation trends

for B20 fuels. The data do, however, suggest the need for more comprehensive studies on B20 (and lower blends) PM that pay careful attention to fuel alterations occurring during/after blending of certified B100 with petrodiesel. To the authors' knowledge, the ASTM test for oxidative stability is carried out typically on neat B100, not the B20 blends. One prior study examined the relationship between B100 fuel stability measurements versus B5 and B20 blends from the same fuel after simulated engine temperature or storage (12 week) conditions. The study concluded that the B5 and B20 blends prepared from "stable" B100 fuels (i.e., that met the IP > 3 hr criterion) generally gave good fuel stability for the B5 and B20 blends.

Table 3. Comparison of neat and aged biodiesel fuel blends: DTT activity magnitude.

For B20:	For B100:
We lack sufficient replicates for neat and 10 hr aging	**5 hr ~ neat**
10 hr is lower than 20 hr	**20 hr is higher than neat**
10 hr is lower than neat	**Neat is lower than B0**
Neat is higher than petrodiesel (B0)	**20 hr ~ B0**
10 hr B20 ~ B0 (but n=1 for 10 hr)	**20 hr B100 is lower than 20 hr B20**

3.2 Fuel Composition – FAMEs

The SIM-mode GCMS results on the FAMEs composition of the oxidized and neat fuels used in the WMBD emissions tests are shown in Figure 9, Figure 10, and Figure 11. Of interest is the degree to which the concentration of the unsaturated FAMEs in the fuel were altered due to exposure of the B100 fuel to accelerated oxidation conditions for 5, 10 or 20 hours. Figure 9 first shows the saturated FAMEs concentrations were unaffected by accelerated oxidation over 20 hours, as expected. In contrast, Figure 10 shows the concentrations of the three unsaturated FAMEs—methyl oleate (C18:1), methyl linoleate (C18:2) and methyl linolenate (C18:3)—did decrease with oxidation time, to varying degrees. Figure 11 compares the relative concentrations (i.e., FAME concentration in oxidized fuel divided by that in neat fuel) of FAMEs, showing larger decreases with increasing oxidation time for the B20 blends compared to B100. Both fuel blends showed the largest change in concentration for linolenic methy ester (C18:3), the FAME with three double bonds, followed by C18:2, then C18:1, as expected. It is unclear why the B20 blends would display such significant changes in FAMEs concentrations with increased oxidation time compared to the B100 fuel (at 20 hours, B20 fuel relative concentrations were 82%, 42% and 18% for C18:1, C18:2 and C18:3, respectively vs 98%, 84% and 73% for B100) unless the process of fuel blending contributed to fuel deterioration in ways significantly different from B100 prior to emissions testing. The DTT results may then reflect how the altered fuels combust differently. It will be interesting to examine the exhaust PM chemical composition for these tests (work that is underway) to better understand these differences between B100 and B20.

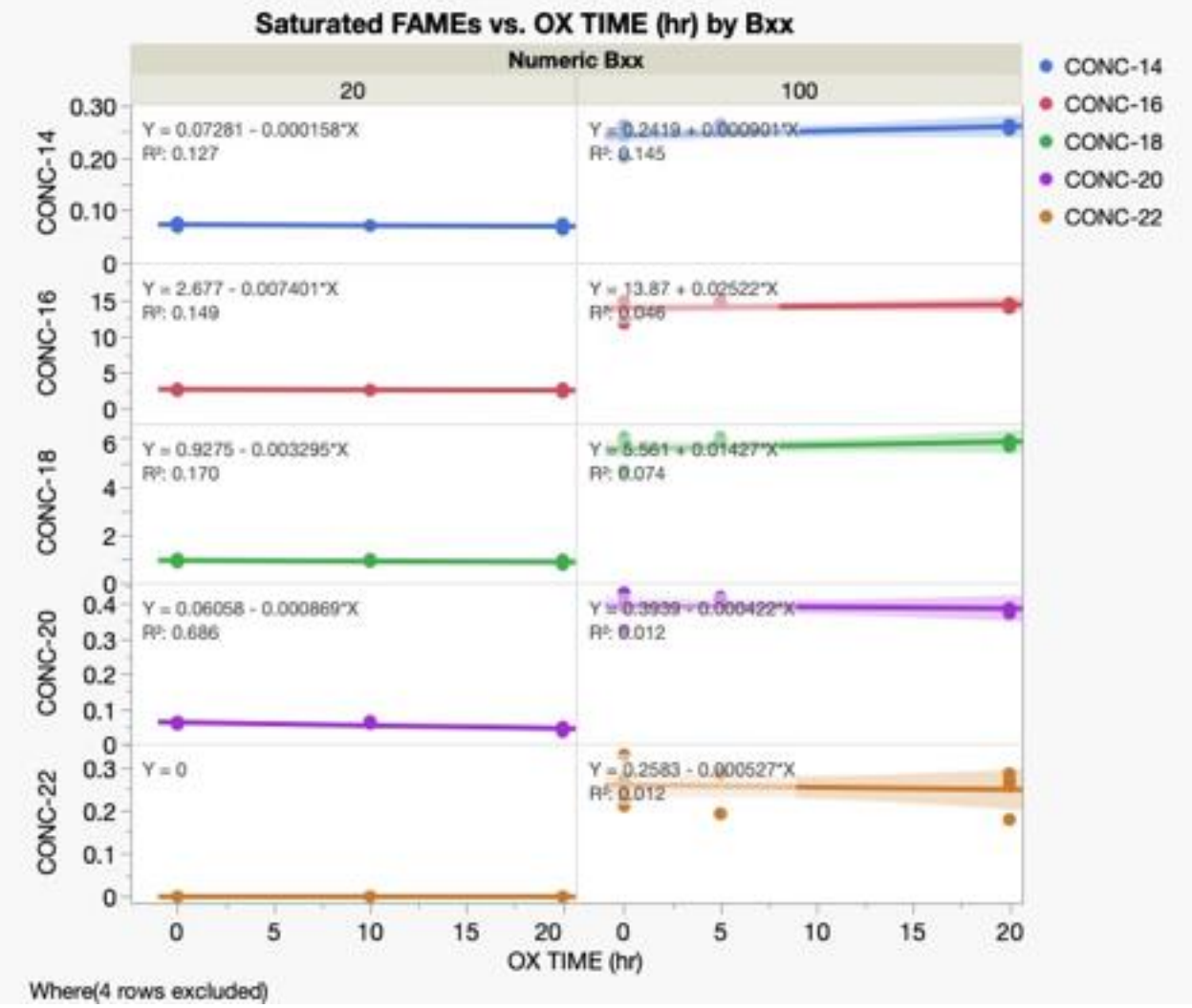

Figure 9. Saturated FAME concentrations in B20 [left] and B100 [right] fuels as a function of oxidation time (hrs).

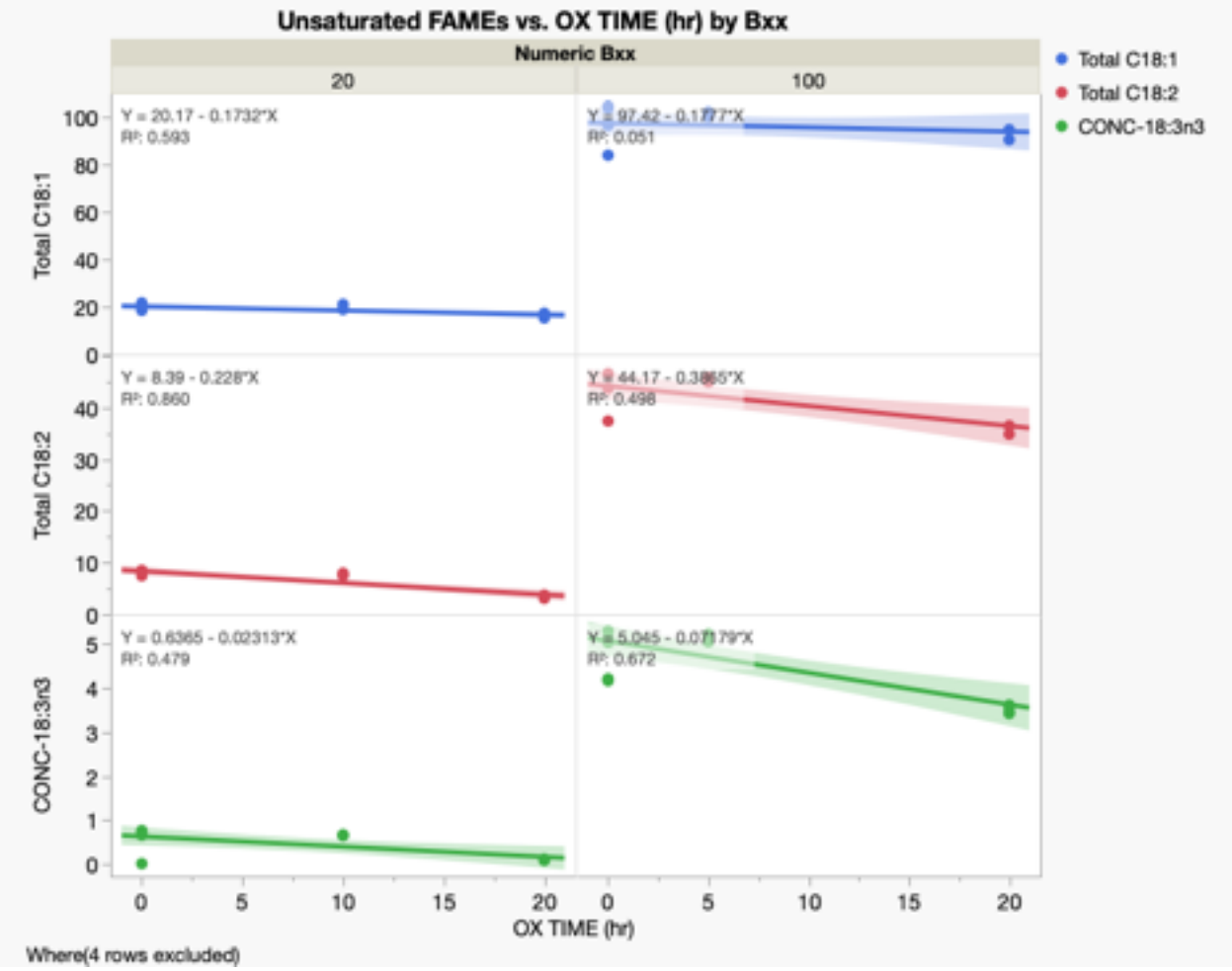

Figure 10. Unsaturated FAME concentrations in B20 [left] and B100 [right] fuels as a function of oxidation time (hrs).

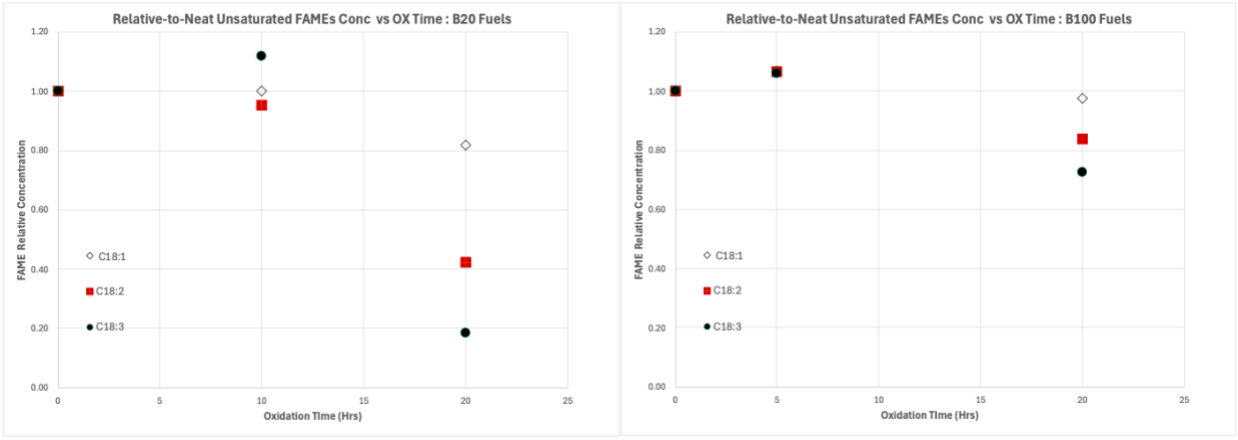

Figure 11. Relative concentration of unsaturated FAMEs in B20 [Left] and B100 [Right] fuels that experienced accelerated oxidation conditions compared to the respective neat fuel. The cis- and trans-isomers were summed for C18:1 and C18:2.

The DTT Activity results compared in Figure 8 and Table 3 indicate the B20 blends had the highest observed activity and therefore possibly the highest potential for ROS formation when these exhaust particles are exposed to cells. It is important to note, however, that the increasing accelerated oxidation time did not show any consistent trend for the B20 blends as would be expected based on Figure 11. Rather, the intermediate oxidation time, 10 hrs, resulted in DTT Activity equivalent to that of the neat B0 fuel and significantly lower than both neat B20 and the 20-hr aged B20. A 20% volumetric blend of biodiesel is chiefly petrodiesel, so we may expect that the combustion particles would be more similar to that of the petrodiesel PM (B0) than the B100 PM. B100 particles, on the other hand, are chiefly comprised of partially oxidized FAMEs, completely different from petrodiesel particles. The neat and 5-hr aged B100 fuels had similar DTT Activity to each other that was lower than the DTT Activity for petrodiesel. In fact, the B100 neat and 5-hr aged fuels showed the lowest DTT Activity measured in this study (Figure 8). The B100 20-hour aged fuel, however, resulted in particles of similar DTT "toxicity" as the neat petrodiesel particles, but still lower than some of the B20 fuels.

The DTT results suggest that more work is needed to understand why the B20 biodiesel blend PM has generally higher potential to form ROS than the B100 fuel. This question is important due to the fact that B20 is one of the widely used biodiesel blends found at the pump. B100, on the other hand, is impractical to use because of its susceptibility to gel formation with cold weather (fuel filter clogging and stalled engines). One limitation of this study was the fact that only one valid emissions test was performed with the 10 hr-B20 fuel, so the lack of replicates complicates data interpretation somewhat. The data also indicate that accelerated oxidation time had very little effect on the B20 fuel's combustion to create toxic particles (Figure 8) but significant effect on fuel FAME composition (Figure 11).

3.3 B100 Induction Period Effects on DTT Activity

Induction period (IP) is a relatively easy measure of the oxidation status of B100 fuel, albeit an expensive measurement to make due to the equipment required (Rancimat or OSI). Given that 20 hr accelerated oxidation of the B100 biodiesel fuel used in this study resulted in higher measured levels of ROS formation potential in both the B100 and B20 exhaust particulate matter samples, it is worthwhile investigating the relationship between IP and DTT Activity. We can compare the BOSS-measured B100 fuels induction period (IP), which should reflect the degree to which original unsaturated FAMEs were lost via lipid oxidation reactions. BOSS results were expected to show *decreasing* IP with increased number of hours at accelerated oxidation conditions. For B100, DTT Assay results were only obtained for neat, 20 hr and 5 hr fuels. For B20 blends (prepared from the same B100 fuels via dilution with petrodiesel), DTT Assay results were only obtained for neat, 20 hr and 10 hr oxidized fuels.

If oxidation of the biodiesel fuel results in formation of oxidation products that are more "toxic" (i.e., in the sense of activating an ROS/immune system biological response) after fuel combustion, then we expect there to be a *positive* relationship between biodiesel fuel oxidation

time and DTT Activity of the associated exhaust PM from the impinger samples. There may, however, be two reasons to not find such a relationship:

1) oxidation products may form polymers that settle out of the fuel and are therefore not present in the fuel or its associated combustion products;
2) the biodiesel FAMEs could be 'over-oxidized' to the point that relatively benign products are formed upon combustion.

Christensen and McCormick (2014) [16] defined 3 phases of biodiesel oxidation (see Figure 12):

Phase 1: Depletion of antioxidant additive – during this phase O_2 consumption via reaction with the biodiesel's unsaturated FAMEs is minimal. Christensen and McCormick 2014 [16] refer to this as the "induction period" or "lag phase".

Phase 2: Here, the antioxidant concentration is so low that O_2 consumption via reaction with unsaturated FAMEs begins to increase exponentially. Reaction products are mainly hydroperoxides and peroxy free radicals.

Phase 3: Antioxidant is essentially depleted and hydroperoxides formation slows down, secondary (2^o) oxidation products form that are both volatile and non-volatile, typically lower molecular weight free acids, ketones and alcohols. Higher molecular weight compounds and polymers can also form.

Chemically, the concentration of hydroperoxides in the oxidized biodiesel fuel remains low until the induction period (IP) is over (Kumar 2017) [42].

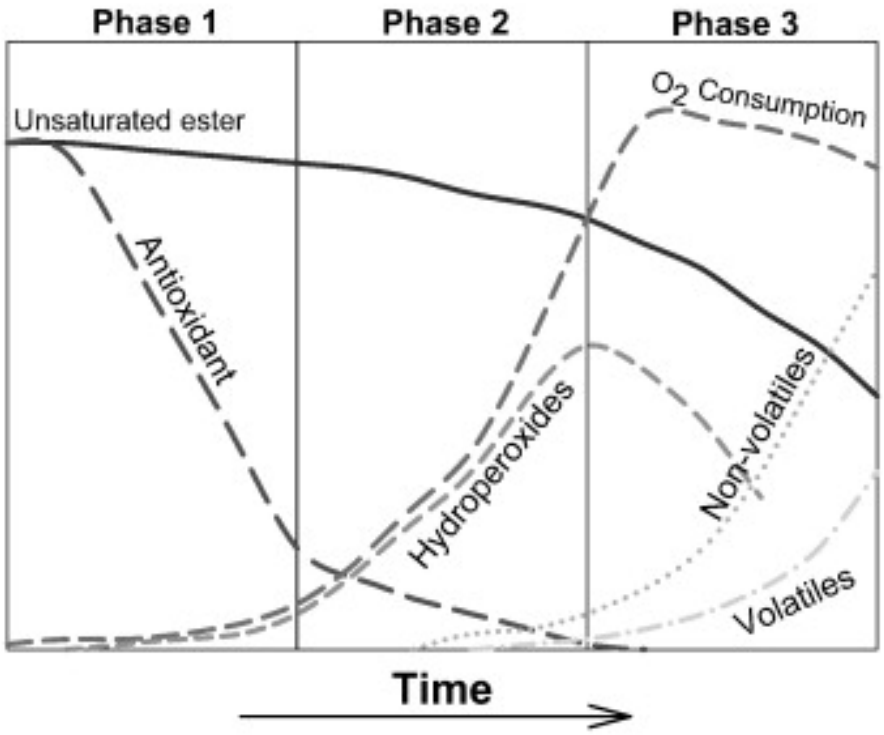

Figure 12. The three phases of oxidation for polyunsaturated FAMEs after Christensen and McCormick (2014) [16].

Figure 13 shows the relationship for the WMBD fuels under the three oxidation conditions versus impinger DTT Assay results. The generally positive relationship (note red arrow and text indicating fuel oxidation increases to the left on the x-axis) is noted: an increase in DTT Activity is observed with increasing fuel oxidation (=shorter induction period). This relationship is obvious for B100, but only holds for the 5-hr aged state (3.15 hr IP) for the B20 blends. It is possible that blending the B100 with petrodiesel to prepare B20 blends affected the IP of the B20 but blend IP was not measured in the BOSS. Further, due to the complexities associated with fuel combustion, the B20 blend showed highly non-linear relationships with DTT toxicity. Blend matters because of significant differences in petrodiesel vs biodiesel combustion properties (biodiesel fuel's bulk modulus is higher such that fuel injection timing is early, compared to B0, creating higher peak temperatures in the engine for biodiesel operation, resulting in higher NOx emissions among other changes in exhaust composition). In other words, due to the complexity of combustion processes as well as the relative changes in FAMEs abundance noted in Figure 11 for B20, it is difficult to tease out the DTT vs IP patterns for B20 which is a mixture of two fuels, one of which (petrodiesel) does not oxidize because it is comprised of n-alkanes (i.e., contains no C=C double bonds that are susceptible to oxidation by O_2). McCormick at al. (2006) [27] examined IP for B100 compared to its B5 and B20 blends, reporting: "*blend stability is dominated by B100 stability*" and "*IP may need to be longer than 3 hr at point of production to ensure stability at point of blending*". That latter conclusion supports the idea that fuel oxidation occurring during Bxx blending should be a concern and it

may have contributed to the variable pattern in DTT "toxicity" reported in the current study for B20 fuels. The magnitude of the effect would of course be highest for the more highly oxidized B100 (e.g., 20 hrs accelerated oxidation). Further, WVO feedstocks may exacerbate fuel stability and oxidation trends in fuel blends—including contributing to ROS formation potential—due to metal-catalyzed reactions such as Fenton's Reaction (Equation [1]) that tend to be more likely when fuel is handled more.

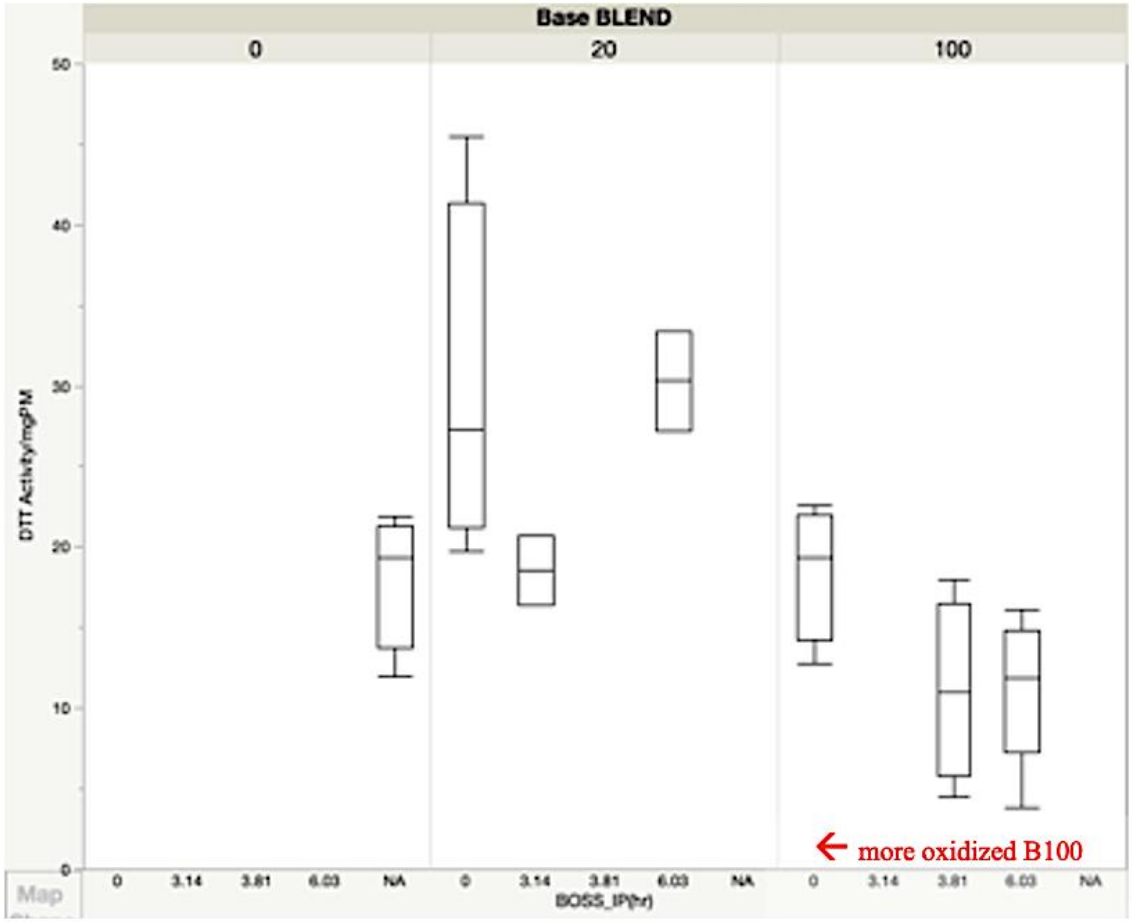

Figure 13. Results for White Mountain Biodiesel (WMBD) Fuel B100 sample induction period (*x*-axis) and DTT Activity (*y*-axis) based on exhaust PM impinger samples after fuel combustion in a light-duty diesel engine. The three sub-panels of each plot are for the different Bxx blends. IP for the B20 blends was assumed equal that of the corresponding B100 fuel. Note that *higher* values of induction period (BOSS_IP(hrs), *x*-axis) correspond to *less oxidized* fuel (i.e., the neat fuel (0 hours of accelerated oxidation and presence of original concentration of antioxidant additive in fuel) had a ~6 hr IP) whereas the fuels oxidized for 20 hr had IP = 0.

3.4 DTT Assay Sanity Check: "PM Activity" Results WMBD vs UCONN Samples

Ben Rukavina's 2014-2015 DTT Assay results for the UCONN biodiesel samples (Holmén et al. 2017) [47]—using both soybean and waste vegetable oil feedstocks and 5 volumetric blends

with petrodiesel, but no accelerated oxidation—show a similar range of DTT Activity (Figure B4) when raw data are normalized to the concentration of PM in the impingers. The agreement was good between the two different analysts and two sets of biodiesel fuels tested on the same engine, but under different drive cycles and laboratory personnel (for emissions testing and DTT Assay). It is also interesting to note the similarly high variability in DTT Assay measurements by both analysts—this is likely due to reagent quality, correction using daily assay blanks and variability in pipetting very small volumes of impinger samples both in DTT Assay and in the Drop Method to determine PM concentration of impinger samples.

With respect to fuel composition, the UCONN unsaturated FAME ratios were different for the C18:2 to C18:1 (linoleate to oleate) ratio, but similar for the C18:3 to C18:2 (linolenate to linoleate) ratio as shown in Figure 14. The trends with oxidation status (OX3 = 5 hr; OX1 = 20hr) clearly shows lower ratios of the unsaturated FAME with more double bonds for both WMBD fuel blends (blue circles, Figure 14).

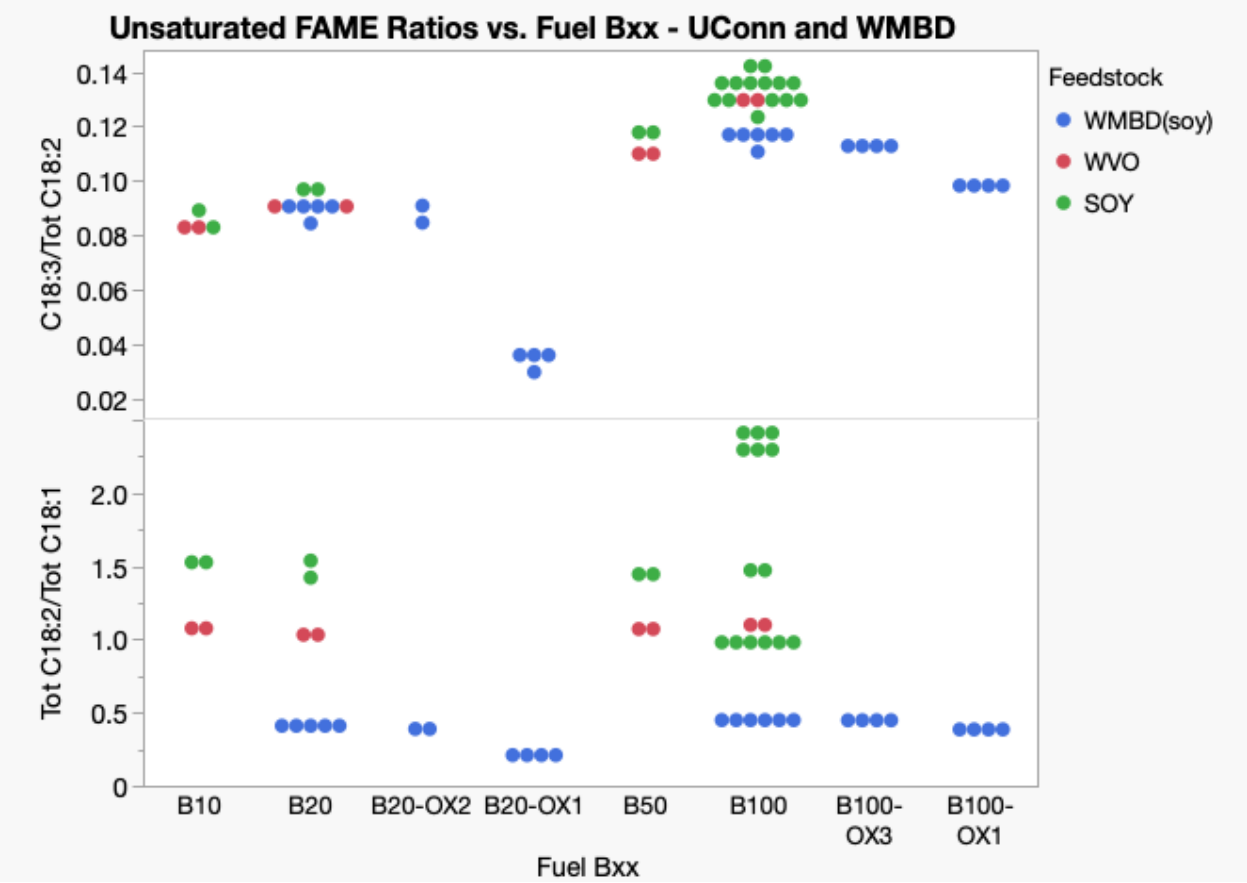

Figure 14. Two ratios of unsaturated FAMEs for fuels studied here (B20 and B100) and in prior work with UCONN biodiesel blends (B10, B20, B50 and B100) of soybean (SOY) and waste vegetable oil (WVO) feedstock biodiesel. Linolenate-to-linoleate [upper panel] and linoleate-to-oleate [lower panel]. Biodiesel feedstock indicated by color: Blue = White Mountain Biodiesel (this study), Red = UCONN waste vegetable oil and Green = virgin soybean oil (prior work).

5.0 Conclusions

The more highly oxidized B20 and B100 fuels (i.e., accelerated oxidation for 20 hours) resulted in the highest DTT Activity for the B100 tests and the highest measured in the study (but also equivalent to the B20 neat fuel's DTT Activity) when that same 20-hr oxidized B100 was used to prepare a 20% biodiesel blend. Further, in this study the highest tendency to form reactive oxygen species, as measured using the abiotic DTT assay, was for the B20 biodiesel fuels, not neat petrodiesel. Importantly, for the B100 fuel PM samples only, not B20, there was a notable inverse relationship between the storage stability (opposite of degree of fuel oxidation) of the biodiesel fuel as measured by induction potential (IP) and the ROS formation potential: higher DTT Activity was noted for the B100 fuels with the lowest IP (= most oxidized neat B100 fuel; 20 hr accelerated oxidation).

The GCMS FAMEs concentration, by contrast, decreased most for B20 fuels, showing the expected largest decrease for the most highly unsaturated FAME, linolenic (C18:3) methyl ester. Both blends showed measurable reductions in unsaturated FAMEs concentrations only at 20 hr of accelerated oxidation, suggesting Phase 3 in the Christensen and McCormick (2014) [16] oxidation scheme (Figure 12) was achieved in this study. Thus, future experiments on the stability of various biodiesel feedstocks could employ the accelerated oxidation techniques used in this study. The results here also caution future researchers to carefully examine FAMEs concentration decreases as well as oxidation product formation as biofuels age in storage and as they are handled in the laboratory. With further study, it should be possible to relate B20 and lower blend fuel composition to predict particle relative "toxicity" under a given set of combustion conditions. Examination of exhaust PM composition to identify possible species associated with higher DTT Activity is on-going.

References

1) Siddharth, Jain and M.P. Sharma (2010). “Stability of biodiesel and its blends: A review.” Renewable and Sustainable Energy Reviews. **14**: 667-678.

2) Schober et al. (2004) “The impact of antioxidants on biodiesel oxidation stability.” Europen Journal of Lipid Science and Technology. 106: 382-389.

3) Osterstrom, et al. (2016). “Oxidation Stability of Rapeseed Biodiesel/Petroleum Diesel Blends.” Energy and Fuels. **30**: 344-351

4) US Energy Information Administration (EIA) (2023) Domestic renewable diesel capacity could more than double through 2025. https://www.eia.gov/todayinenergy/detail.php?id=55399. Accessed October 24, 2023

5) ASTM D6751-15ce1, Standard Specification for Biodiesel Fuel Blend Stock (B100) for Middle Distillate Fuels, ASTM International, West Conshohocken, PA, 2015, www.astm.org

6) Knothe, G. (2007). "Some aspects of biodiesel oxidative stability." Fuel Processing Technology **88**(7): 669-677.

7) Knothe G. (2008). “Designer” biodiesel: optimizing fatty ester composition to improve fuel properties. *Energy Fuels*; 22: 1358–1364.

8) Didem Özçimen and Sevil Yücel (2011). “Novel Methods in Biodiesel Production.” Biofuel: Engineering Process Technology. August 1, 2011. DOI: 10.5772/18750.

9) Lapuerta et al. (2007) “Effect of biodiesel fuels on diesel engine emissions.” Energy and Combustion Science 34: 198-223.

10) Karavalakis, G.; Boutsika, V.; Stournas, S.; Bakeas, E. Biodiesel emissions profile in modern diesel vehicles. Part 2: Effect of biodiesel origin on carbonyl, PAH, nitro-PAH and oxy-PAH emissions. Sci. Total Environ. 2011, 409 (4), 738−747.

11) Machado Correâ,S.; Arbilla,G. (2008) Carbonyl emissions in diesel and biodiesel exhaust. Atmos. Environ. 42 (4), 769−775.

12) Payri,F.;Bermuḍez,V.R.;Tormos,B.;Linares,W.G. Hydrocarbon emissions speciation in diesel and biodiesel exhausts. Atmos. Environ. 2009, 43 (6), 1273−1279.

13) Kasumba, J., N. Fukagawa, and B. A. Holmeń (2019) Fuel Composition Effects on Carbonyls and Quinones in Particulate Matter from a Light-Duty Diesel Engine Running Biodiesel Blends from Two Feedstocks. Energy & Fuels, 33 (2), 1133-1145.

14) Farahani, M., D.J.Y.S. Pagé, M.P. Turingia, B.D. Tucker (2009) Storage Stability of Biodiesel and Ultralow Sulfur Diesel Fuel Blends. J. Energy Resources Technology, Transactions of the ASME, December 2009, Vol 131, 041801-1 – 041801-6.

15) Waynick, J. Andrew (2005) Characterization Of Biodiesel Oxidation And Oxidation Products. CRC Project No. AVFL-2b Task 1 Results. Prepared for Coordinating Research Council, Alpharetta, GA. August 2005. NREL/TP-540-39096.

16) Christensen, E. and R. L. McCormick (2014). "Long-term storage stability of biodiesel and biodiesel blends." Fuel Processing Technology 128: 339-348.

17) Donaldson, K.; Li, X. Y.; MacNee, W. Ultrafine (nanometre) particle mediated lung injury. *J. Aerosol Sci.* **1998**, *29* (5-6), 553–560.

18) Donaldson, K.; Stone, V.; Seaton, A.; MacNee, W. Ambient particle inhalation and the cardiovascular system: potential mechanisms. *Env. Health Perspect* **2001**, *109 Suppl 4*, 523–527.

19) Langrish, J. P.; Bosson, J.; Unosson, J.; Muala, A.; Newby, D. E.; Mills, N. L.; Blomberg, A.; Sandström, T. Cardiovascular effects of particulate air pollution exposure: time course and underlying mechanisms. *J. Intern. Med.* **2012**, *272* (3), 224–239.

20) Sacks, J. D.; Stanek, L. W.; Luben, T. J.; Johns, D. O.; Buckley, B. J.; Brown, J. S.; Ross, M. Particulate Matter-Induced Health Effects: Who Is Susceptible? *Environ. Health Perspect.* **2011**, *119* (4), 446–454.

21) Samet, J. M.; DeMarini, D. M.; Malling, H. V. BIOMEDICINE: Do Airborne Particles Induce Heritable Mutations? *Science* **2004**, *304* (5673), 971–972.

22) Sawyer, K.; Mundandhara, S.; Ghio, A. J.; Madden, M. C. The Effects of Ambient Particulate Matter on Human Alveolar Macrophage Oxidative and Inflammatory Responses. *J. Toxicol. Environ. Health-Part -Curr. Issues* **2010**, *73* (1), 41–57.

23) Schrooten, L.; De Vlieger, I.; Lefebre, F.; Torfs, R. Costs and benefits of an enhanced reduction policy of particulate matter exhaust emissions from road traffic in Flanders. *Atmos. Environ.* **2006**, *40* (5), 904–912.

24) Swanson, K. J.; Madden, M. C.; Ghio, A. J. Biodiesel exhaust: The need for health effects research. *Environ. Health Perspect.* **2007**, *115* (4), 496–499.

25) Swanson, K. J., N.Y. Kado, W.E. Funk, J.D. Pleil, M.C. Madden, A. J. Ghio. Release of the Pro-Inflammatory Markers by BEAS-2B Cells Following In Vitro Exposure to Biodiesel Extracts. *Open Toxicol. J.* **2009**, *3*, 8–15.

26) Donaldson, K.; Tran, L.; Jimenez, L. A.; Duffin, R.; Newby, D. E.; Mills, N.; MacNee, W.; Stone, V. Combustion-derived nanoparticles: a review of their toxicology following inhalation exposure. *Part. Fibre Toxicol.* **2005**, *2*, 10.

27) McCormick, R.L., T.L. Alleman, S. Westbrook, J. A. Waynick, S. Porter (**2006**) Oxidation Stability of Biodiesel and Biodiesel Blends. Conference presentation, ASTM Toronto, June 2006. NREL/PR-540-40356.

28) Wiltsee. *Urban Waste Grease Resource Assessment*; National Renewable Energy Laboratory: Golden, CO, **1998**; p 70. And: *Used and Waste Oil and Grease for Biodiesel* - eXtension http://www.extension.org/pages/28000/used-and-waste-oil-and-grease-for-biodiesel (accessed Oct 19, **2015**).

29) (29) Kasumba, J. and B.A. Holmén (**2016**) Nonpolar Organic Compound Emission Rates for Light-Duty Diesel Engine Soybean and Waste Vegetable Oil Biodiesel Fuel Combustion. Energy & Fuels, 30 (11), 9783–9792. DOI: 10.1021/acs.energyfuels.6b01582

30) Li, Q. F.; Wyatt, A.; Kamens, R. M. Oxidant generation and toxicity enhancement of aged-diesel exhaust. *Atmos. Environ.* **2009**, *43* (5), 1037–1042.

31) Charrier, J. G.; Anastasio, C. On dithiothreitol (DTT) as a measure of oxidative potential for ambient particles: evidence for the importance of soluble transition metals. *Atmospheric Chem. Phys.* **2012**, *12* (19), 9321–9333.

32) Jariyasopit, N.; McIntosh, M.; Zimmermann, K.; Arey, J.; Atkinson, R.; Cheong, P. H. Y.; Carter, R. G.; Yu, T. W.; Dashwood, R. H.; Simonich, S. L. M. Novel Nitro-PAH Formation from Heterogeneous Reactions of PAHs with NO2, NO3/N2O5, and OH Radicals: Prediction, Laboratory Studies, and Mutagenicity. *Environ. Sci. Technol.* **2014**, *48* (1), 412–419.

33) Donaldson, K.; Tran, L.; Jimenez, L. A.; Duffin, R.; Newby, D. E.; Mills, N.; MacNee, W.; Stone, V. Combustion-derived nanoparticles: a review of their toxicology following inhalation exposure. *Part. Fibre Toxicol.* **2005**, *2*, 10.

34) Biswas, S.; Verma, V.; Schauer, J. J.; Cassee, F. R.; Cho, A. K.; Sioutas, C. Oxidative Potential of Semi-Volatile and Non Volatile Particulate Matter (PM) from Heavy-Duty Vehicles Retrofitted with Emission Control Technologies. *Environ. Sci. Technol.* **2009**, *43* (10), 3905–3912.

35) Cheung, K. L.; Ntziachristos, L.; Tzamkiozis, T.; Schauer, J. J.; Samaras, Z.; Moore, K. F.; Sioutas, C. Emissions of Particulate Trace Elements, Metals and Organic Species from Gasoline, Diesel, and Biodiesel Passenger Vehicles and Their Relation to Oxidative Potential. *Aerosol Sci. Technol.* **2010**, *44* (7), 500–513.

36) Surawski, N. C.; Miljevic, B.; Ayoko, G. A.; Elbagir, S.; Stevanovic, S.; Fairfull-Smith, K. E.; Bottle, S. E.; Ristovski, Z. D. Physicochemical Characterization of Particulate Emissions from a Compression Ignition Engine: The Influence of Biodiesel Feedstock. *Environ. Sci. Technol.* **2011**, *45* (24), 10337–10343.

37) Stevanovic, S.; Miljevic, B.; Surawski, N. C.; Fairfull-Smith, K. E.; Bottle, S. E.; Brown, R.; Ristovski, Z. D. Influence of Oxygenated Organic Aerosols (OOAs) on the Oxidative Potential of Diesel and Biodiesel Particulate Matter. *Environ. Sci. Technol.* **2013**, *47* (14), 7655–7662.

38) Miljevic, B.; Fairfull-Smith, K. E.; Bottle, S. E.; Ristovski, Z. D. The application of profluorescent nitroxides to detect reactive oxygen species derived from combustion-generated particulate matter: Cigarette smoke – A case study. *Atmos. Environ.* **2010**, *44* (18), 2224–2230.

39) Fukagawa, N. K.; Li, M.; Poynter, M. E.; Palmer, B. C.; Parker, E.; Kasumba, J.; Holmén, B. A. Soy Biodiesel and Petrodiesel Emissions Differ in Size, Chemical Composition and Stimulation of Inflammatory Responses in Cells and Animals. *Environ. Sci. Technol.* **2013**, *47* (21), 12496–12504.

40) Reed, Jack Elliot (2021) The Effects of Oxidized Biodiesel Fuel on Fatty Acid Methyl Ester Composition and Particulate Matter Emissions from a Light-Duty Diesel Engine. MS Thesis, University of Vermont, Civil & Environmental Engineering. Available at https://scholarworks.uvm.edu/graddis/1344/

41) European Committee for Standardization. EN15751: "Automotive fuels—Fatty Acid Methyl Ester (FAME) fuel and blends with diesel fuel: Determination of oxidation stability by accelerated method." 2014.

42) Kumar (2017). "Oxidative Stability of Biodiesel: Causes, Effects, and Prevention." Fuel **190** (2017): 328-350.

43) Yaakob, Z., et al. (2014). "A review on the oxidation stability of biodiesel." Renewable and Sustainable Energy Reviews 35: 136-153.

44) Obadiah, A., Kannan, R., Ramasubbu, A., Kumar, S.V. "Studies on the effect of antioxidants on the long-term storage and oxidation stability of Pongamia pinnata (L.) Pierre biodiesel." Fuel Process & Technol. Volume 99. 2012. Pages 56–63.

45) Risom, L.; Moller, P.; Loft, S. Oxidative stress-induced DNA damage by particulate air pollution. *Mutat. Res.-Fundam. Mol. Mech. Mutagen.* **2005**, *592* (1-2), 119–137.

46) Cho, A. K.; DiStefano, E.; You, Y.; Rodriguez, C. E.; Schmitz, D. A.; Kumagai, Y.; Miguel, A. H.; Eiguren-Fernandez, A.; Kobayashi, T.; Avol, E.; et al. Determination of four quinones in diesel exhaust particles, SRM 1649a, an atmospheric PM2.5. *Aerosol Sci Technol* **2004**, *38*, 68–81.

47) Holmén, B.A., B. Rukavina, J. Kasumba, N. K. Fukagawa (**2017**) Reactive oxidative species and speciated particulate light-duty engine emissions from diesel and biodiesel fuel blends. Energy & Fuels, 31 (8), pp 8171–8180. DOI: 10.1021/acs.energyfuels.7b00698

Appendix A. Drop Method Standard Operating Procedure

This SOP consists of two documents as of February 2021, both reproduced here.

HOLMÉNGROUP STANDARD OPERATING PROCEDURE

Drop method for Quantifying PM Suspension Concentration.

Written By: Brad Haire, January 19, 2011
Date of Last Edits: April 19, 2011

Table of contents:

I. Introduction
II. Required Materials and Equipment
III. Safety considerations
IV. STEP-BY-STEP PROCEDURE
V. ANALYSIS Using Excel Template File
VI. Quality Control
VII. Ordering Supplies

I. Introduction:

The purpose of this document is to summarize the experimental procedures used to quantify the mass concentration of particles in liquid impinger samples that contain Armfield diesel engine raw exhaust. In these experiments, mass concentration is expressed as milligrams of engine exhaust particulate matter per milliliters (mL) of impinger suspension (mg/mL).
The methods used to collect the impinger samples are found in a separate SOP entitled, "Armfield Engine SOP_10FEB2011_TF" available from Prof Holmén.

II. Required Materials and equipment:

Figure A1 through Figure A8 are photographs of some of the key supplies and equipment needed to carry out these procedures.

II.1. Small steel cylinder with flat end for creating Aluminum foil weighing cups 1 1/4 inches long and 3/8-inch diameter (Figure A1, A)

II.2. Regular weight aluminum foil (Reynolds Wrap or equivalent) Forceps – Millipore (blunt tip) (Figure A1, B)

II.3. Falcon 1007 Petri dishes 60x15mm for creating foil lined Petri dishes. (Figure A1, C&D)

II.4. Large solid aluminum cylinder with flat end ½ inch long, 2 inch diameter for making the bottoms of the foil lined Petri dished (Figure A1, E)

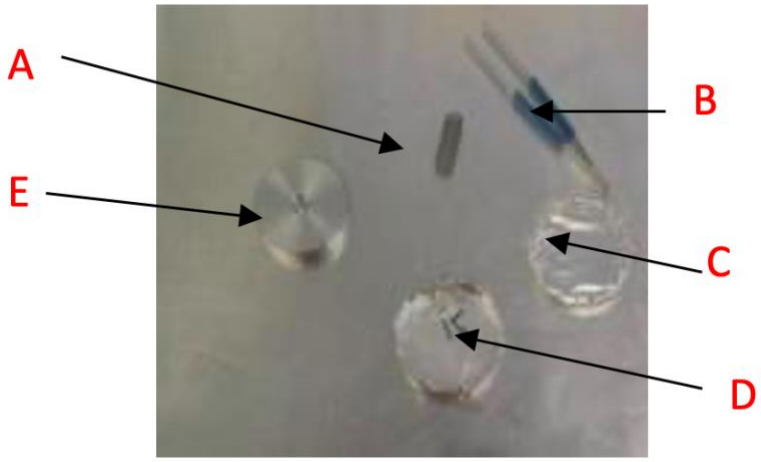

Figure A1. Key supplies. A: Small cylinder. B: Millipore Forceps. C: Foil lined Petri dish top. D: Foil lined Petri dish, bottom. E: Large cylinder.

II.5. Fisher scientific Vortex-Genie vortexer to mix up the suspensions (Figure A2).

Figure A2. How to hold impinger sample on vortexer.

II.6. Desiccator with fresh Drierite Anhydrous calcium sulfate Desiccant for drying out the solvent in the suspensions.(blue = fresh; pink = water-saturated) (Figure A3).

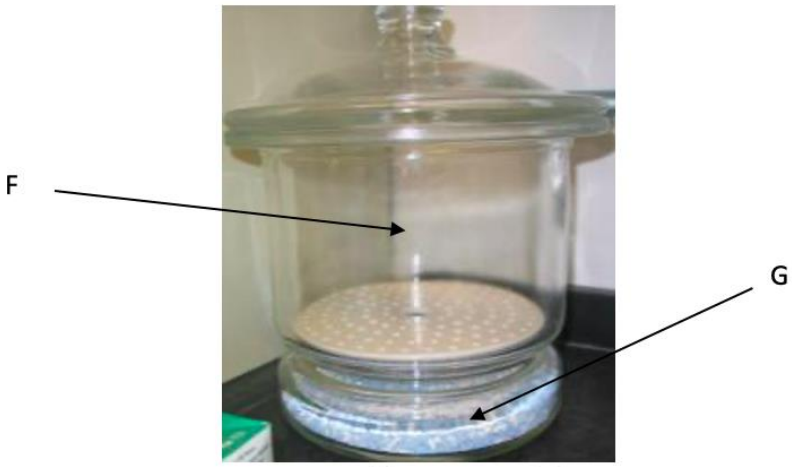

Figure A3. Desiccator (F) with desiccant (G).

II.7. Cahn Model C-33 Microbalance in Coy Chamber (Figure A4).

Figure A4. Coy Chamber (left)with Cahn Microbalance (right).

II.8. 100 µL Drummond Pipette with glass tips for aliquoting suspensions (Fukagawa lab) (no model number) (Figure A5).

Figure A5. 100 uL Drummond Micro Pipetter (top) and tip (bottom) with ruler for scale.

II.9. Nitrogen blowdown station for concentrating ethanol samples (Figure A6).

Figure A6. Ultra-pure Nitrogen tank (Right) and Nitrogen blowdown station (Left).

II.10. ETS Automatic humidity controller (model #514C) instrument for measuring the humidity in the coy chamber (Figure A7).

Figure A7. The ETS control box associated with the humidity conditions in the Coy Chamber.

II.11. Dickson logger model TRJ320 for measuring the temperature and Relative humidity in the Coy Chamber (Figure A8).

Figure A8. Dickson logger.

III. SAFETY CONSIDERATIONS

The major safety hazard associated with this procedure is ethanol which is the solvent for the suspensions. The chemical is toxic and flammable, so caution should be used when containers are outside the hood. It is impotent that the ethanol be kept out of the eyes as it will cause severe irritation. Nitrogen poses little risk as long as the blowdown station remains in the hood. The MSDS for all chemicals are in the Laboratory Safety Notebook.

III.1. Glass Pipette tips to be disposed of in approved "Broken Glass" waste container

III.2. Safety glasses and gloves are to be worn at all times while chemicals are in use, and gloves should be worn while creating aluminum weighing cups and aluminum foil lined Petri dishes to keep oils from hands from adding mass.

IV. STEP-BY-STEP PROCEDURE

The "Drop Method" is used to determine the particle mass (PM) concentration in a suspension based on removing a 100uL aliquot of that suspension to a pre-weighed aluminum foil cup, letting that aliquot dry completely in a dessicator and/or using nitrogen blowdown (when ethanol is not the solvent)], and post-weighing the cup after complete dryness is reached. The difference in mass is ratioed to the volume of aliquot removed to determine the suspension's PM mass concentration.

It should be noted that it is critically important to reproducibly mix the suspension prior to removal of the aliquot. It is also important to make sure the aliquot is reproducibly delivered to the foil cup (no particles or liquid remain in the glass pipet tip). The procedure is performed in triplicate, and the data is averaged to give final concentration. **Heat should not be used to dry the aliquot of suspension because it can lead to loss of the more volatile particle components and result in poor reproducibility**.

The procedure is divided into five distinct operations –

IV.4.1. Preparation of Petri dishes and aluminum foil weighing cups (The Petri dishes are used to store the foil cups and prevent cross-contamination between sample aliquots), and preweighing the aluminum weighing cups.

IV.4.2. Mix and aliquot the sample;

IV.4.3. Blowdown and desiccation;

IV.4.4. Post-weigh foil cups

IV.4.5. Data Analysis using Excel template file.

IV.4.6. Quality Control

IV.4.7. Ordering Supplies.

IV.1. Preparation of Petri Dishes and Aluminum Foil Weighing Cups

Note: Gloves *MUST* be worn!

IV.1.1. Prepare triplicate aluminum foil-lined **Petri dishes** for each sample to be measured (to store one Petri dish per Drop Method "cup").

IV.1.1.1. Place a ~2.5 inch square of aluminum foil on top of Petri dish opening dull side up (because the shiny side has oils used in manufacturing).

IV.1.1.2. For the cover of the Petri dish, place opening of bottom over opening of top and press in gently to prevent damage to the Petri dish.

- Remove excess aluminum foil and flatten the foil using the bottom of the Petri dish, to make a flat disk and minimize the chances of the cover falling off.

IV.1.1.3. For the bottom of the Petri dish, take the large metal Cylinder and press in gently, while removing excess aluminum foil so that the aluminum foil reaches only the top edge of the Petri dish.

IV.1.1.4. Label Petri dish cover and inside foil with permanent marker. For example, if there are 5 samples total, 15 Petri dishes will be lined and numbered consecutively, 1 through 15; this is for self reference to keep track of which sample is which.

IV.1.2. Prepare Triplicate aluminum foil weighing cups for each sample to be measured (Aluminum foil regular weight). (see Figure A8).

IV.1.2.1. Take the small metal cylinder and place flat end in center of a ~ 1 inch square piece of aluminum foil dull side up so that the sample will not come in contact with the oils used in manufacture.

IV.1.2.2. Gently wrap bottom of cylinder in foil

IV.1.2.3. Press cylinder flat end on heavy duty aluminum covered lab bench.

IV.1.2.4. Place newly formed cup into aluminum foil lined Petri dish created in step IV1.1.

Figure A9. Aluminum foil cup top view (top) and side view (bottom) with ruler for scale.

IV.1.3. Coy chamber/ CAHN C-33 Microbalance Preparations

The Cahn Microbalance (1 µg sensitivity) is used instead of an analytical balance because of the sensitivity of the instrument. The microbalance has a limit of 0.001 micrograms and a maximum of around 200 micrograms.

IV.1.3.1. General Pointers for the use of the Cahn-33 Microbalance:

- No vinyl gloves should be used at any time while using the balance to prevent static buildup on the gloves from adversely affecting the balance.
- The Polonium-210 strips both inside the measurement chamber and outside are an anti static agent.
- The stirrup with weighing pan tends to get stuck all the way down when the 100 and 200 milligram weights are added, but bringing the door down sharply frees the jam, but if the stirrup is not jammed bring the door down softly.
- The acceptable range of relative humidity (RH%) is 30-40% ± 5% this is regulated by, during times of high humidity like summer, turning on the ETS controller's dehumidifier function with fresh desiccant. During times of low humidity the ETS controller's humidifier switch is turned on with a open container of water inside the Coy Chamber.
- The acceptable range for the temperature is ideally 20-23°C ±2 °C, not regulated by the coy chamber.

This next set of instructions is to calibrate the balance and acquire an initial RH% for the coy chamber. Then the pre wight of the Aluminum Foil weighing cups is taken so that the mass of the cup may be removed from the final mass.

IV.1.3.2. Record temperature from D1 logger

- Data from loggers Downloaded into computer biweekly. File names contain DX, where X is the logger number, and the date the data was downloaded.

IV.1.3.3. Record %RH (ETS box on bench)

IV.1.3.4. Weigh 50 mg Calibration weight by placing weight on middle of scale to evenly distribute weight on scale.

- Wait until mass reading is stable for 10 to 15 seconds so that measurements will be as consistent as possible
- Record mass three times on drop method logsheet at 10 second intervals, so that the drift of the scale is taken into account.

IV.1.3.5. repeat step IV.1.3.4 for 100 mg calibration weight

IV.1.3.6. repeat step IV.1.3.4 for 200 mg

IV.1.4. repeat step IV.1.3.4 to Pre-weigh aluminum foil weighing cups

A.1.4.1. Replace foil cups in foil-lined Petri dishes on bench make sure that the cup is returned to the same Petri dish it was taken from.

A.1.4.2. If not all cups are being used on the same day, make copies of the log sheet.

IV.2. Mix and aliquot the PM suspension.

IV.2.1 Place glass tip, the correct100mL tip had blue rings on it, on 100 µL Drummond Micropipettor.

IV.2.1.1. Set the micropipettor display to "00.0" by moving the switch on top to unlock, then using the textured knob until 00.0 is lined up in display window.

IV.2.1.2. Place switch into locked position.

IV.2.1.3. Attach a clean glass tip to the end of the Drummond Pipettor. The orange bore should be inserted until it is on bottom blue ring.

IV.2.2 Vortex suspension in amber bottle at an angle for 30 seconds. (Figure A2)

- Vary the position of the amber bottle by rotating with wrist in a clockwise manner while vortexing. The base of the bottle should be in contact with the vortexer at all times.

IV.2.3 Full An aluminum cup by:

IV.2.3.1. Open the cap of the amber bottle containing the suspension vortexed in step 6

IV.2.3.2. Place impinger tip into suspension half an inch from the bottom.

IV.2.3.3. Plunge plunger up and down 5 times to help expel air bubbles

IV.2.3.4. Place tip of pipette over aluminum cup in the Petri dish labeled 1.

IV.2.3.5. Depress plunger quickly.

IV.2.3.6. Check that the glass tip has no particle residue on the walls if particulate matter visible, redo cup from step IV.1.2.

IV.2.4 Repeat sampling step IV.2.3 for the second and third cups of the triplicate with the same pipette tip using the cups numbered sequentially.

IV.2.5 Repeat steps IV.2.1 through IV.2.3 using different cups until all samples are dispensed

IV.2.6 Tap side of each individual Petri dish to check for leaks, if cup doesn't move it is most likely due the liquid of a leaking cup adhering the cup to the foil lining of the Petri dish replace with new pre-weighed foil cup and repeat step IV.2.3 through IV.2.6 until three leak free replicates exist.

IV.3. Blowdown and Desiccation of Samples:

IV.3.1. Blowdown sample to visual dryness with nitrogen at 5 Psi, and using the needle valves to adjust flow rates, if solvent is not ethanol or any other easily evaporated solvent

such as water, because of the time it takes water to evaporate, means that the sample might not be completely dry.

- For ethanol samples precede to step IV.3.2 as the evaporation of ethanol is quick enough to not require this step.

IV.3.2. Place sample in while in Petri dish in desiccator overnight with lids ajar, or if enough samples exist stacked so that the cups are covered by the Petri dish above it, and the top layer has the lids ajar.

IV.3.3. repeat step IV.1.3.4 for 200mg calibration weight

IV.3.4. repeat step IV.1.3.4 for 100mg calibration weight

IV.3.5. repeat step IV.1.3.4 for 50mg calibration weight

IV.4. Post-Weigh Aluminum Foil Cups.

IV.4.1. At least 24 hours later reweigh the calibration weights, and post the samples. The data should go in the same logsheets as the pre-weights for the cups.

IV.4.1.1. repeat step IV.1.3

IV.4.1.2. Repeat step IV.1.4 to post-weigh aluminum foil weighing cups.

IV.4.1.3. Repeat steps IV.3.3 through IV.3.5

V. DATA ANALYSIS USING EXCEL TEMPLATE FILE

The object of the data analysis is the determination of the suspension's PM mass concentration, standard deviation, and coefficient of variation (CV%) of the measurements. The calculations are doneusing a Microsoft Excel spreadsheet template with the formulas arranged in a manner that as long as the data in input correctly, the results are calculated automatically. The Spreadsheet for data computation and recording has the filename "Drop_Method_Summary" with the date of the last revision appended, and can be found at fs1.cems.uvm.edu\holmengroup \Brad_All_Files\Impinger Data.

V.1. Copy the "template" tab, and paste it directly to the right of the "template" tab in the same excel file.

V.2. Rename template tab to "I#_date" I stands for Impinger and # is the ID number of the impinger samples as recorded on the sampling logsheet and the label on the amber bottle, and "date" is the month, day, and year the data was being put into the spreadsheet (ie.19Apr2011).

V.3. Add as many rows as needed for all data to include one row for each cup, 3 rows per impinger.

V.4. Copy all formulas into the appropriate cells.

V.5. Input pre-weigh dates into the green column marked date

V.6. Input post-weigh dates into peach colored "date" column

V.7. Input volume aliquoted into ‘Volume of sample (mL)’ column

V.8. Input Preweigh masses into green ‘Pre weight substrate (mg)’ columns with each measurement of a single cup going horizontally

V.9. Input post weigh data into ‘Post weight substrate with sample (mg) with each measurement of a single cup going horizontally

V.10. Input RH% from the ETS, temperature from the D1 Dickson logger, and military time each taken at the end of each sample’s measurement into the appropriate columns.

V.11. Input beginning and ending calibration weights into the calibration weight section, along with the time of each measurement.

V.12. Plot run conditions temperature vs. time and humidity vs. time.

V.13. Formulas used in calculations in spreadsheet

V.13.1. Average= average values of each replicate measurement

V.13.2. STDEV= standard deviation of each replicate measurement

V.13.3. Standard deviation/average X 100= CV%

VI. QUALITY CONTROL

VI.1. Every 10th sample triplicate should be a method blank, which is a sample of ethanol placed in the amber bottle them measured. This is followed by a solvent blank which is just the ethanol (or other solvent) taken from the original container and touches no glassware besides a beaker for measuring the sample out..

VI.2. Method blank preparation, pour ethanol, from the same source as used for the samples, into a clean empty amber bottle, then perform drop method analysis this is to test the cleaning methods.

VI.3. Solvent blank preparations, pour ethanol from storage container into a clean beaker, do not contact any other glassware beyond beaker and Drummond pipette tips. Then perform drop method analysis steps.

VII. ORDERING SUPPLIES

VII.1. Falcon 1007 Petri dishes 60x15mm in a case of 500 $167.70 and Drummond glass bores (tips) 100 pack $17.35, from Fisher Scientific

Regular weight aluminum foil can be purchased from the nearest convenience store.

Preparation, Pre- and Post-Weighing of Aluminum Foil Weighing Cups
Updates to Drop Method for Quantifying PM Suspension Concentration

By Wenyu Zhu

Written on 02/10/2021
Last edit: 02/12/2021

This document describes the specific procedure to be used in the UVM TAQ (Transportation Air Quality) Lab for determining the PM concentrations of biodiesel impinger samples. The full drop method, including data analysis and quality control, is not described here. To see that full SOP, see the document titled "SOP_Drop_Method_BJH_2011.docx". This document shows the methods to (a) make aluminum foil weighing cups, and (b) collect data on the *pre-weight* and *post-weight* of the cups using the Mettler Toledo XPE 26 microbalance at the Colchester Research Facility (CRF) lab of Dr. Thomas Jetton.

1. Required Materials and equipment

(a) Small steel cylinder (diameter of 12 mm) with flat end for creating Aluminum foil weighing cups (known affectionately as "DropMethod cups" or "DM cups").
(b) Regular weight aluminum foil (Reynolds Wrap or equivalent) for making the cups and liner of the 24-well plates.
(c) Heavy duty aluminum foil (Reynolds Wrap or equivalent) for covering of the bench.
(c) Forceps that came with the XPE26 microbalance (on the left of the microbalance).
(d) Regular flat bottom 24-well plates for creating foil-lined holders for the DM cups.
(e) One AA battery-wrapped with Aluminum foil (dull side facing out) for making the bottoms of the foil-lined 24 well-plates.
(f) Desiccator with fresh silica gel in CRF lab (Orange = fresh; Green to black = water-saturated) for drying out the solvent in the suspensions.
(g) Mettler Toledo XPE26 in microbalance room of CRF lab.

2. Prepare aluminum foil weighing cups.

Wipe the aluminum foil **dull side** with ethanol before use if ethanol is the solvent for the PM samples. Make cups and lined 24-well-plates on **Heavy duty** Aluminum foil covered bench (**dull side up**) to avoid possible contamination. Proper PPE is required all the time, but do not use vinyl gloves so as to prevent static electricity buildup on the gloves.

2.1 Prepare at least triplicate aluminum foil-lined 24 well-plates Petri dishes to store Drop Method cups.

(a) Use a ~15 x 10 cm piece of regular aluminum foil to line the cover of the 24 well plate
(b) Loosely wrap the AA battery with a ~2.5 cm inch square of aluminum foil (dull side up) and press in gently into each well to make the liner on the bottom and the inner

wall of each well. Remove excess aluminum foil to allow the aluminum foil to reach only the top edge of the Petri dish).

(c) Label the 24-well plates for self-reference to keep track of which sample is which. The labeling scheme should include Letter and Number of each well in the plate. For example, “A1” is the first cell in upper left corner.

2.2 Prepare Triplicate aluminum foil weighing cups for each sample to be measured (Aluminum foil regular weight).

Perform cup-making using gloved hands! The cups should only be handled with forceps after they are constructed—i.e., during pre- and post-weighing/handling in and out of desiccator.

(a) Take the small metal cylinder and place its flat end in the center of a ~ 1.5 cm square piece of aluminum foil **dull side up** so that the sample will not come in contact with the oils used in manufacture.

(b) **Gently** wrap bottom of cylinder in foil.

(c) Press cylinder flat end down on heavy duty aluminum covered lab bench with sufficient pressure to make a flat bottom on the cup, but taking care to not pierce the lower edge of the cup. (That lower edge is possible leakage point and all cup bottoms should be checked visually before proceeding).

(d) Use a razor or other cutting device (scissors) to trim the height of the cup to be 5 ± 2 mm.

(e) Carefully remove the cup from the mold and the place newly formed cup into one of the aluminum foil-lined wells in the 24-well plate.

3. Use of XPE26 microbalance to pre- and post- weigh the cups

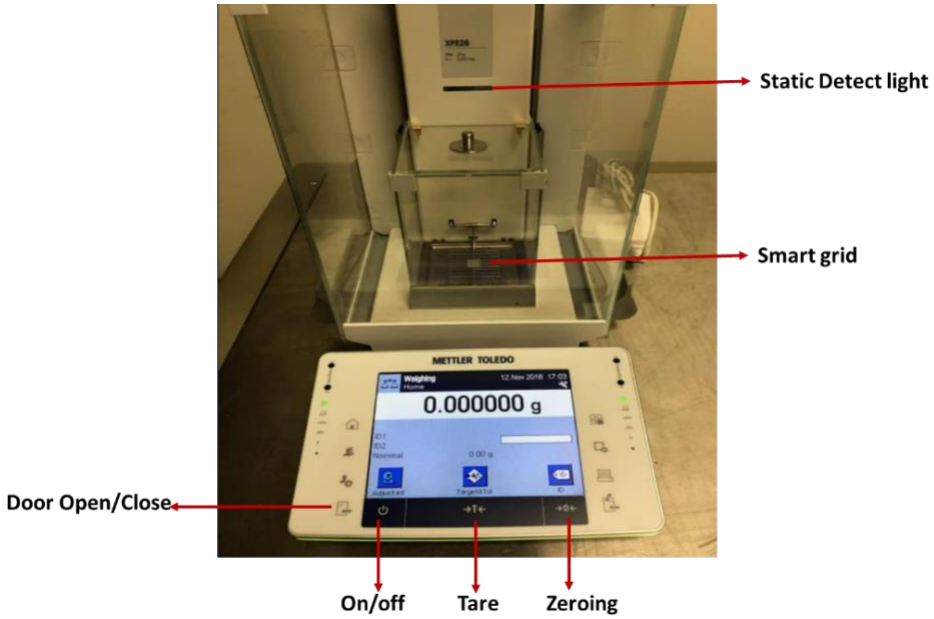

Figure A10. An example photo of Mettler Toledo XPE26.

Figure A10 is a photo of XPE26 microbalance. It is important to make sure the microbalance is working under good status, and it is the user's responsibility to evaluate the status of the microbalance and adjust/align the microbalance if needed following the details given by the XPE26 manual.

To use the microbalance correctly, it is essential to note that:

(a) On the right rear of the microbalance, there is a Level indicator/Leavel sensor (a balance bubble) to correct horizontal alignment. Before turn on the machine, the position of the bubble of the indicator should be firstly checked. Only start using the machine when the bubble is in the center. Once the level indicator detects incorrect leveling, the front panel would turn to Red with a warning text. Follow the manual 3.6 to correctly level the balance.

(b) The machine has **a static detect light**, and when it is shining with **blue light** this suggest the existence of static electricity. Check thoroughly from the tools to the containers to find the source of the static electricity and restart the weighing after the static electricity is removed.

(c) As an important quality control process, the microbalance should be regularly calibrated/checked using standard calibration weights of 50 mg, 100 mg and 200 mg, respectively.

(d) A Dickson logger model TRJ320 is used to record the temperature and RH% (Relative Humidity) in the weighing room. The readings/changes of the logger should be recorded throughout the measurement. The acceptable range of relative humidity (RH%) is 30-40% ± 5% and the acceptable range for the temperature is ideally 20-23°C ±2 °C.

(e) The XPE microbalance is very sensitive, and any movement of the table can alter its reading. It is suggested that after the DM cup is put on the smart grid, try to record the reading in your logsheet or lab notebook located on a different table to avoid disturbing the microbalance table. Throughout the weighing process, it is necessary to work in a gentle and careful way. Sometimes air turbulence may occur due to the air conditioning system, wait and only restart the weighing process when the reading of the microbalance is stable.

(f) The cups are only 12 mm in diameter, it is important to avoid spilling of samples and their tendency to flip over during the weighing process. Cover the bench surface around the microbalance using heavy duty aluminum foil (**dull side up**) to avoid contamination in the event DM cups are accidentally dropped when using the forceps to move the cups.

3.1 Regular calibration of the XPE26 microbalance.

Detailed calibration procedures as below:

(a) Turn on the microbalance by pressing the power button, wait a while until the reading of **0.000 mg** appears on the display panel. If the reading is not 0.000 mg, press "zeroing" to allow the reading to go to 0.000 mg.

(b) Always use the forceps to carefully put the standard weight on the smart grid (the weighing pan). Weigh 50 mg standard weight on the center of the smart grid to evenly distribute weight on scale.

(c) Wait until mass reading is stable for 10 to 15 seconds so that measurements will be as consistent as possible. Record the weight 3 times, at 10 sec intervals.

(d) Take off the 50 mg standard weigh, and then repeat (b) and (c) for each of the 100 mg and 200 mg calibration weights.

(e) Weigh each standard weight for at least 3 times, so that the drift of the scale is taken into account.

3.2 Pre-weigh the aluminum foil DM cups with XPE26 microbalance

(a) Make sure the 24-well plate are correctly labeled and the DM cups are correctly put in their specific wells.

(b) Carefully remove the top of the 24-well plate and use the forceps to gently take out one DM cup from its well, and weigh the cup following the same method as described in (a) to (d) of **3.1**.

(c) After each weighing, use forceps to carefully put the cup back to its well.

(d) Weigh each cup for at least 3 times and record the readings.

(e) Record the changes of temperature and RH% from the Dickson logger immediately after each record of cup weight.

(f) Clean the chamber of the microbalance and the bench after use.

3.3 Desiccation of samples before post-weight

Check the color of the silica gel orange and dry the silica gel orange using oven if needed.

(a) Follow Section IV.2, "Mix and Aliquot the PM suspension" of the document, SOP_Drop_Method_BJH_2011, to aliquot the samples into the pre-weighed DM cups.

(b) After all samples are prepared, carefully transfer the 24-well plate to the desiccator. To avoid spilling of samples, the 24-well plate can be first naturally dried (ethanol evaporate quickly) on the bench before any movement.

(c) If ethanol is the solvent, dry the samples in the desiccator for at least 24 hours before re-weight the cups. If other solvent is used, adjust the drying time accordingly.

3.4 Post-weigh the DM cups

(a) Make sure the DM cup samples are sufficiently dried in the desiccator before re-weighing the cups.

(b) Use the forceps to carefully remove the cups without touching the dried PM material on the bottom of the cups to avoid losing sample.

(c) Weigh the cup following the same method as described in (a) to (d) of 3.1.

(d) After each weighing, use forceps to carefully put the cup back into its well.

(e) Weigh each cup for at least 3 times and record the readings.

(f) Record the changes of temperature and RH% from the Dickson logger.

(g) Clean the chamber of the microbalance and the bench after use.

Appendix B. Impinger Data

1.0 DTT Assay – Raw Data

Raw impinger time plots (i.e., Normalized DTT remaining concentration (micromolar) vs. experimental time (min)) for each Assay Blank, impinger and PQN positive control are show in Figure B1 with the best-fit line for all replicates. The observed steeper slopes for the positive control (Phenanthrenequinone, PQN) are as expected compared to the nearly flat line for the Assay Blank negative controls. Exhaust PM impinger samples show slopes between these control endpoints.

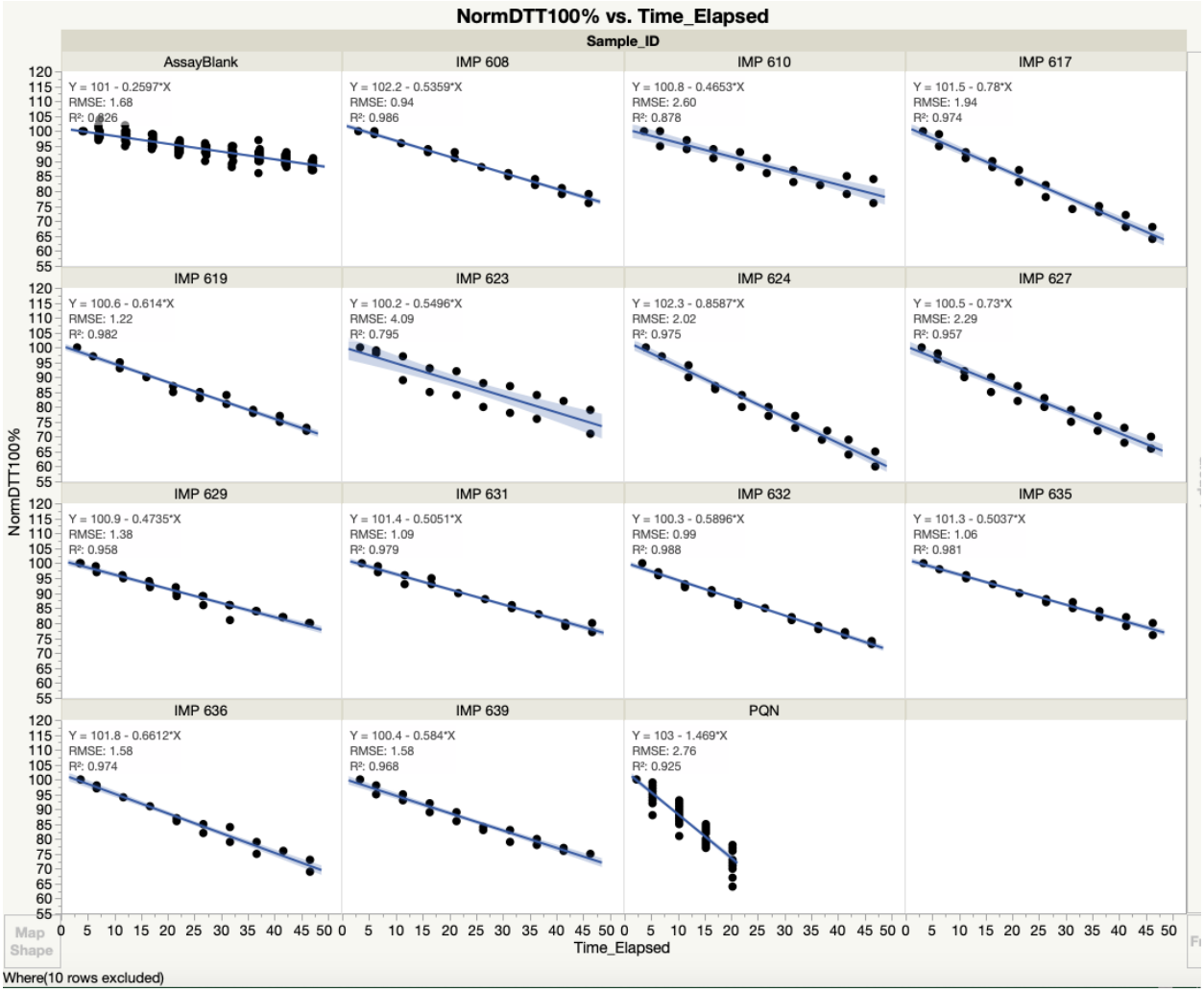

Figure B1. Normalized DTT assay experimental time points (TP1 to 100) for each PM impinger, Assay Blank and PQN quality control sample. Plots show linear fit by sample. Steeper slopes indicate higher consumption of DTT and therefore higher ROS formation potential.

Comparison of the individual sample DTT Assay raw results in the overlay plot of Figure B2 shows the Assay Blank at the top (with the shallowest slope) and PQN positive control at the

bottom (with steepest slope). It is interesting to note that there appear to be three “groups” of impinger samples and their data fall between the negative and positive control data (Figure B2).

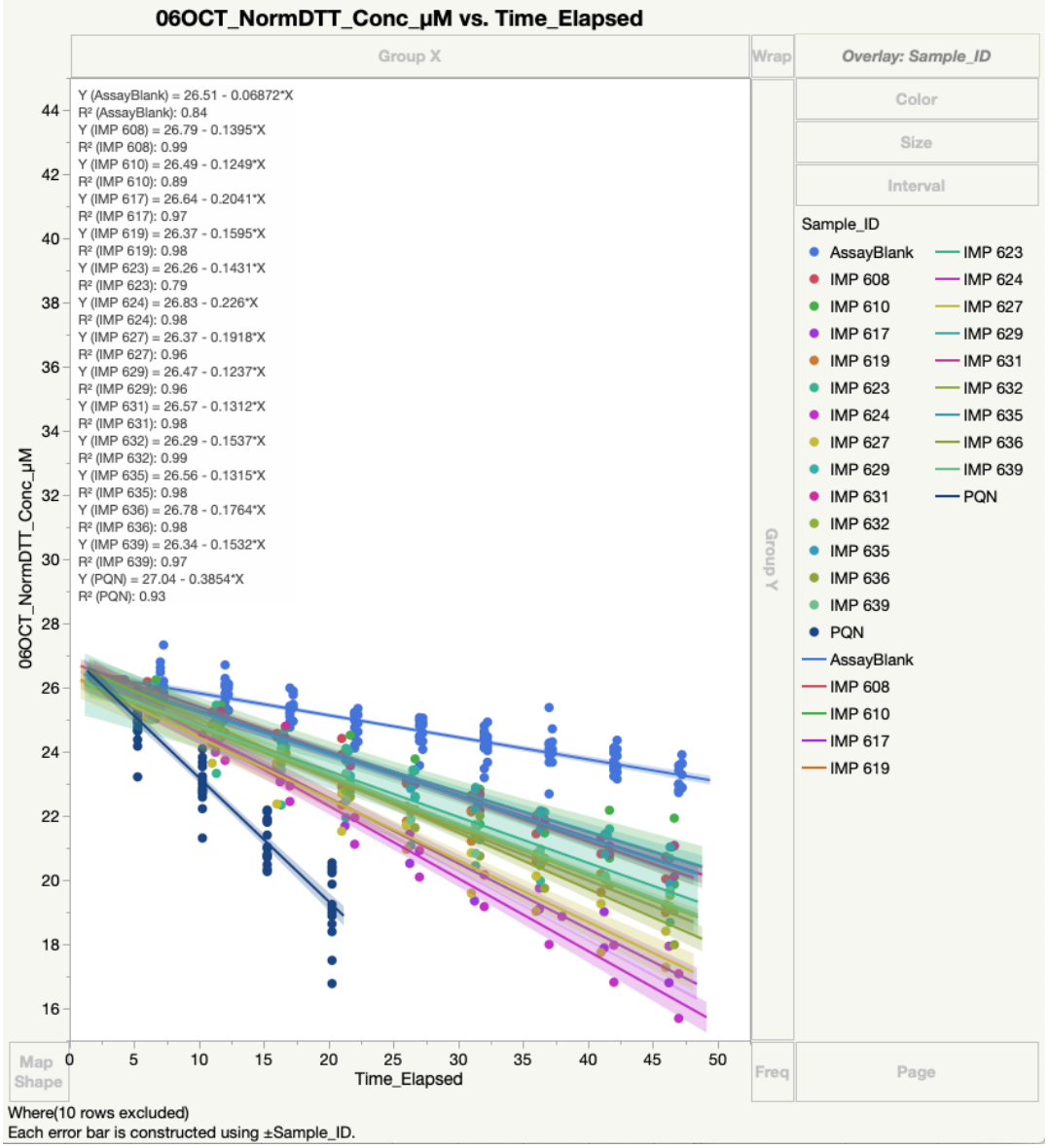

Figure B2. Raw data normalized to TP1=26.235 uM DTT, the theoretical value initially in each cuvet at start of the DTT assay. JMP 14.2 best fit results show in text at top left for each impinger and control sample.

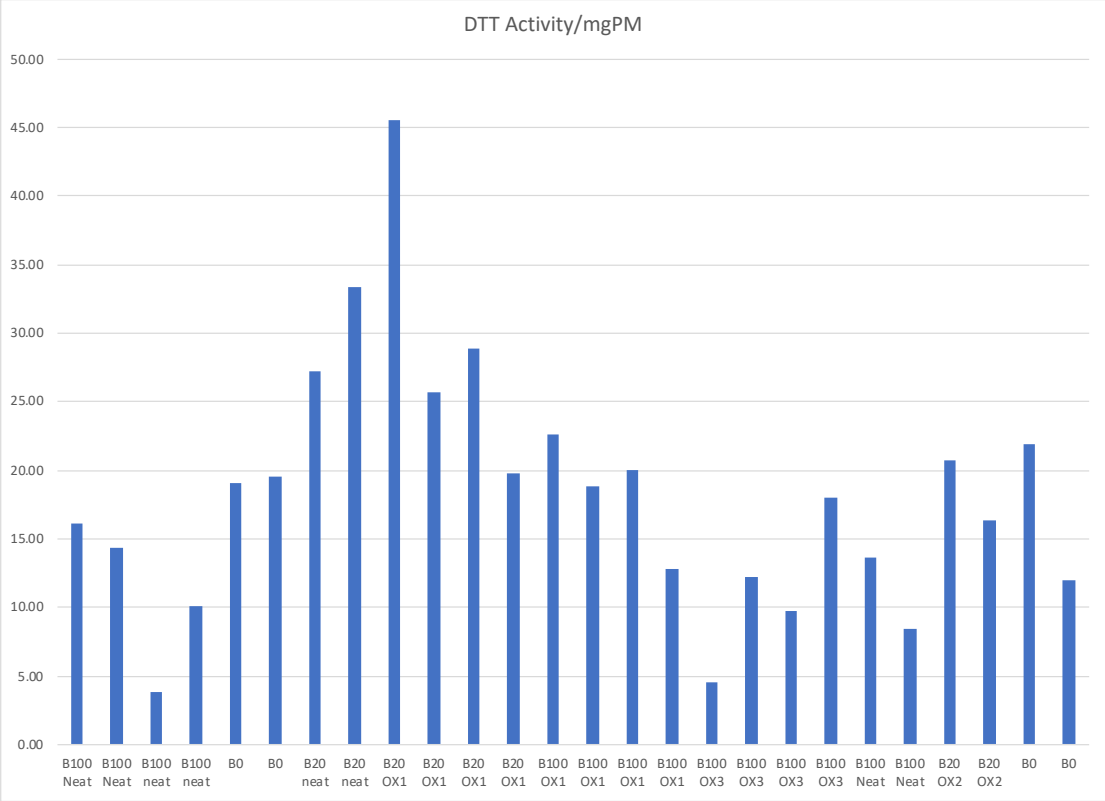

Figure B3. DTT Activity (nmol DTT/min/microgram PM) for individual duplicate DTT Assays for each impinger labelled by the fuel blend (Excel chart).

1.1 Comparison to Prior DTT Assay Work in TAQ Lab

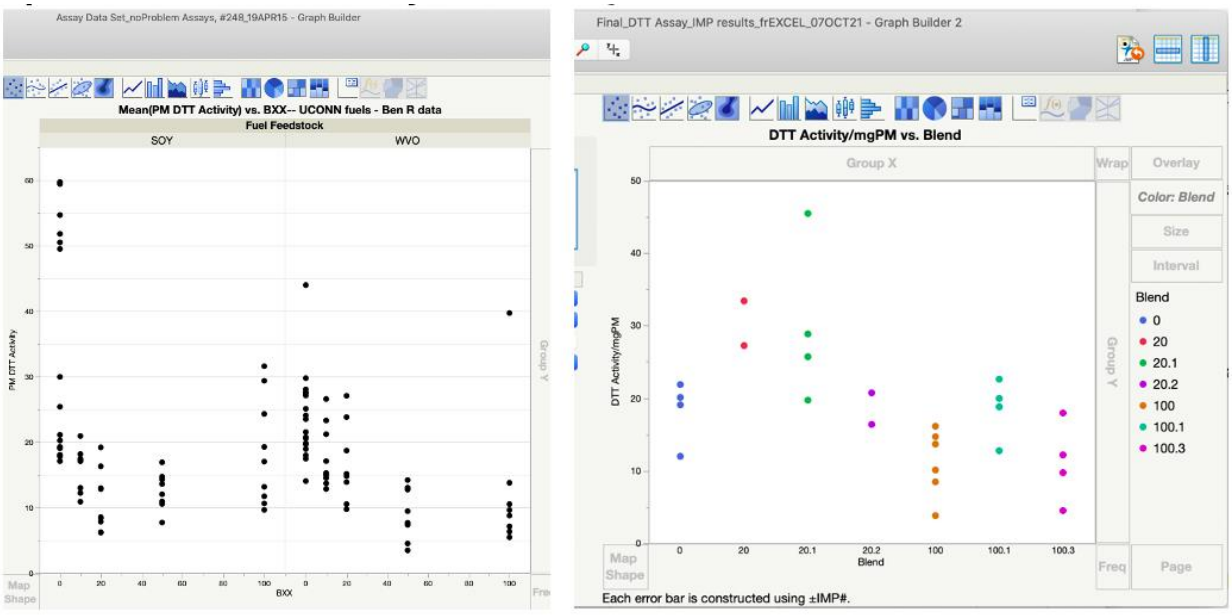

Figure B4. DTT Activity for PM impinger samples from two exhaust emissions studies with the same VW engine, but different driving cycles and biodiesel fuel sources. UCONN fuels (left) and WMBD fuels (right). Note that the X-axis labels in right panel refer to fuel oxidation states—".1" means 20 hr, ".2"= 10 hr and ".3"= 5 hr for each base fuel blend (B20 or B100). [Example: 20.2 means the B20 fuel underwent 10 hr accelerated oxidation]. The UCONN fuels in left panel did not undergo accelerated oxidation and a different petrodiesel source fuel (Trono Fuels) was used to mix the Bxx blends.

1.2 Intrasample Variability in DTT Assay Data

Figure B5 shows the same data for the WMBD oxidized fuel blends, but plotted differently to enable color to represent fuel OX state. The data at condition OX1 (20 hr) for B20 fuel, IMP #623 and #624 have large error bars and contribute to the fact that the means between the different fuel oxidation states were not statistically different at the 95% confidence level (Figure B5). Further, Figure B6 ANOVA charts show that p-values were improved when the #623 replicate A data were removed from analysis, but there was still no statistical difference between means at various OX levels for B20 at the 95% level (p=0.1155 vs. 0.3589 with all replicates)

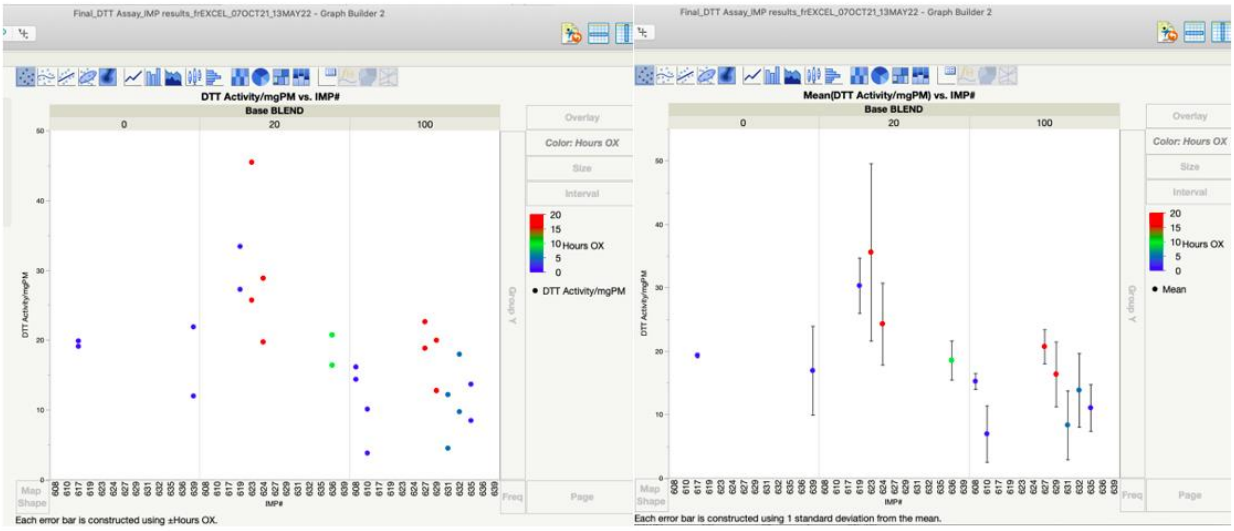

Figure B5. [Left] Individual impinger DTT Activity (nmol DTT/min/mgPM) results, organized by blend with color of circle indicating oxidation time (0=none, 5, 10 or 20 hr). [Right] Same data, but symbol shows mean +/- 1 SD of the duplicate DTT Assay measurements for each impinger. Note the large error bar for impinger #623.

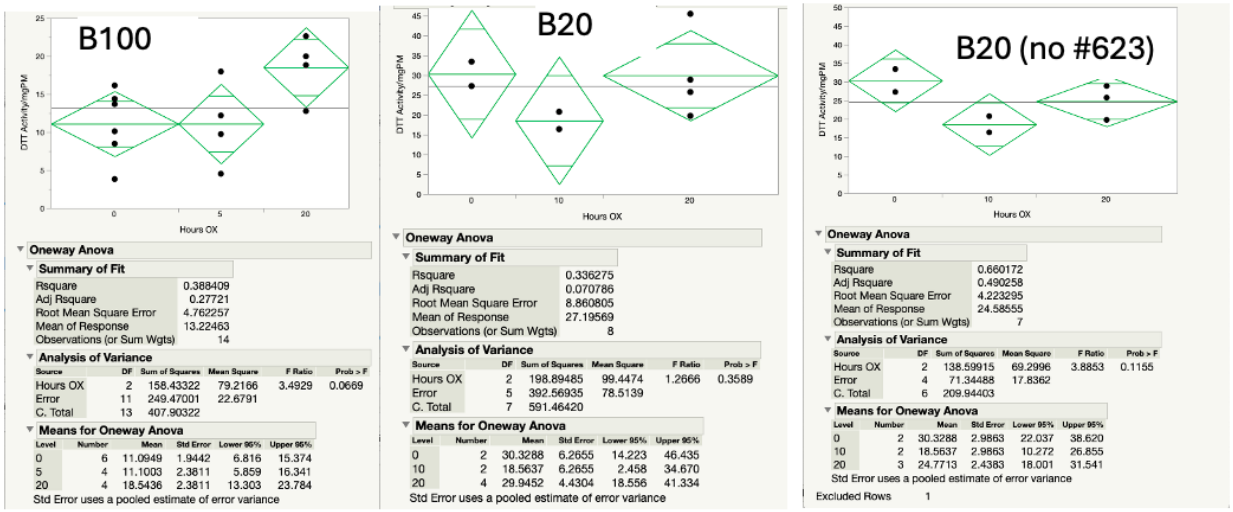

Figure B6. One-way analysis of variance test results for impinger sample DTT Activity by hours of B100 fuel oxidation. [left] B100 fuels; [center] B20 blends; [right] B20 blends, excluding the IMP #623 outlier (replicate A only was removed).

Appendix C. Gas Chromatography – Mass Spectrometry Information

INSTRUMENT CONTROL PARAMETERS: Instrument #1

C:\MSDCHEM\1\METHODS\SIMMODE_BRITT_SLB-IL100_FAME_ACQ_08SEP21_JR9SEPT.M

Control Information

Sample Inlet : GC
Injection Source : GC ALS
Mass Spectrometer : Enabled

6890 GC METHOD

OVEN
Initial temp: 50 °C (On) Maximum temp: 230 °C
Initial time: 1.00 min Equilibration time: 0.50 min
Ramps:

#	Rate	Final temp	Final time
1	10.00	140	1.00
2	3.00	160	0.00
3	10.00	220	3.00
4	0.0(Off)		

Post temp: 0 °C
Post time: 0.00 min
Run time: 26.67 min

FRONT INLET (SPLIT/SPLITLESS)
Mode: Splitless
Initial temp: 240 °C (On)
Pressure: 12.65 psi (On)
Purge flow: 20.0 mL/min
Purge time: 2.00 min
Total flow: 23.9 mL/min
Gas saver: Off
Gas type: Helium

COLUMN 1
Capillary Column
Model Number: Supelco SLB-IL100
SLB-IL100 Polar FAMES
Max temperature: 230 °C
Nominal length: 30.0 m
Nominal diameter: 250.00 um
Nominal film thickness: 0.20 um
Mode: constant flow
Initial flow: 1.5 mL/min
Nominal init pressure: 12.65 psi
Average velocity: 45 cm/sec
Inlet: Front Inlet
Outlet: MSD
Outlet pressure: vacuum

GC Injector
Front Injector:
Sample Washes 2
Sample Pumps 2
Injection Volume 1.00 microliters
Syringe Size 10.0 microliters
PreInj Solvent A Washes 2
PreInj Solvent B Washes 2
PostInj Solvent A Washes 2
PostInj Solvent B Washes 2
Viscosity Delay 0 seconds
Plunger Speed Fast
PreInjection Dwell 0.00 minutes
PostInjection Dwell 0.00 minutes

MS ACQUISITION PARAMETERS

General Information
Tune File : btune.U
Acquisition Mode : SIM

MS Information
Solvent Delay : 6.50 min
EM Absolute : False
EM Offset : 0
Resulting EM Voltage : 1764.7

SIM PARAMETERS

Group #	Start Time (min)	Mass Ion 1	Mass Ion 2	Mass Ion 3	Mass Ion 4	Mass Ion 5	Mass Ion 6	Dwell Time
1	0.0	74.10	87.10	143.20	242.30			25
2	12.2	74.10	87.10	143.20	256.00			25
3	13.5	74.10	87.10	143.20	270.30			25
4	15.5	74.10	87.10	143.20	298.30			25
5	16.6	55.10	69.20	74.10	97.10	264.30	296.20	19
6	17.4	41.10	55.10	67.20	81.10	95.10	294.10	19
7	18.6	74.10	87.10	143.20	326.00			25
8	19.0	55.10	67.10	79.10	95.10	292.00		20
9	19.5	74.10	87.00	143.10	340.00	354.00		20

THERMAL AUX 2
Use: MSD Transfer Line Heater
Description:
Initial temp: 230 °C (On)
Initial time: 0.00 min

#	Rate	Final temp	Final time
1	0.0(Off)		

Figure C1. GCMS Selected Ion Monitoring (SIM) acquisition parameters.

Table C1. GCMS quantitation method (scan mode).

FAME ID	Target Ion m/z	Qualifier Ion Q1 m/z	Qualifier Ion Q2 m/z	Qualifier Ion Q3 m/z	Retention Time (minutes)
C14:0	74	87	143	55	10.785
C16:0	74	87	143	75	13.768
C18:0	74	87	143	75	17.026
C18:1 trans-9	55	69	74	97	17.615
C18:1 cis-9	55	69	74	83	17.620
C18:2 trans-9,12	67	81	95	82	18.600
C18:2 cis-9,12	67	81	95	55	18.307
C20:0	74	74	75	143	20.958
C18:3n3	79	95	67	93	20.255
C22:0	74	87	75	55	23.404

Table C2. Unsaturated FAME concentrations relative to NEAT fuel (OX = 0).

	B20				B100		
OX TIME (HR)	**C18:1**	**C18:2**	**C18:3**	**OX TIME (HR)**	**C18:1**	**C18:2**	**C18:3**
0	1.00	1.00	1.00	**0**	1.00	1.00	1.00
5				**5**	1.07	1.07	1.06
10	1.00	0.95	1.12	**10**			
20	0.82	0.42	0.18	**20**	0.98	0.84	0.73

Reported based on ng/uL concentrations measured in diluted fuel samples.

1.0 Calibration Curves for Individual FAMEs using SIM Analysis

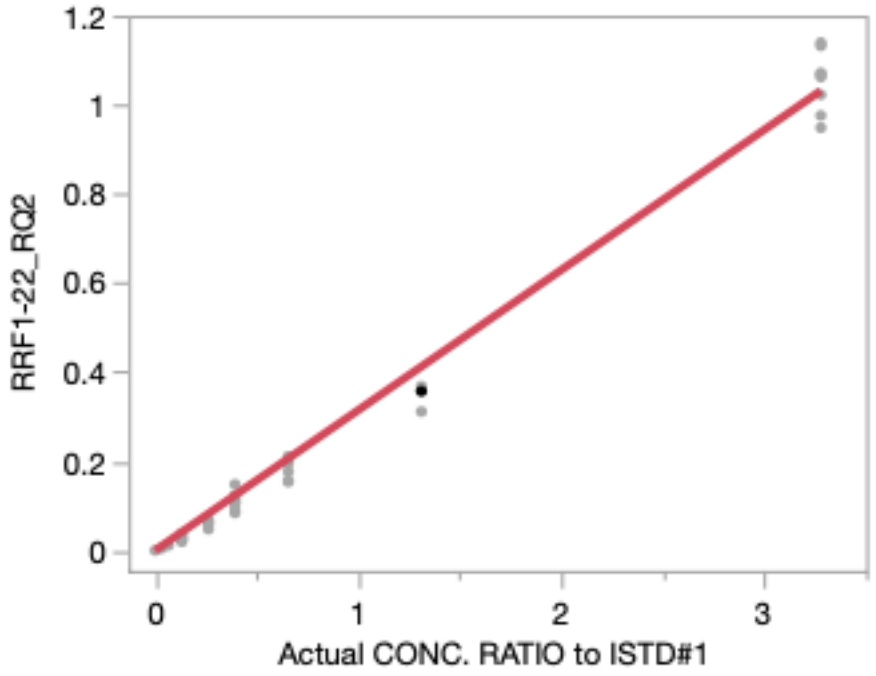

Figure C2. Calibration curve for C22:0 FAME, methyl behenate.

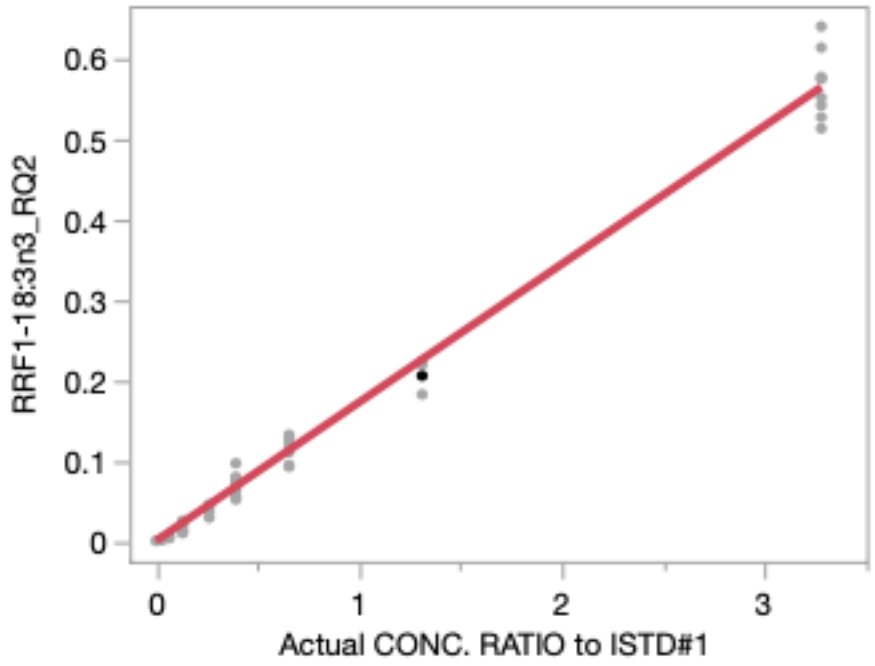

Figure C3. Calibration curve for C18:3 FAME, methyl linolenate.

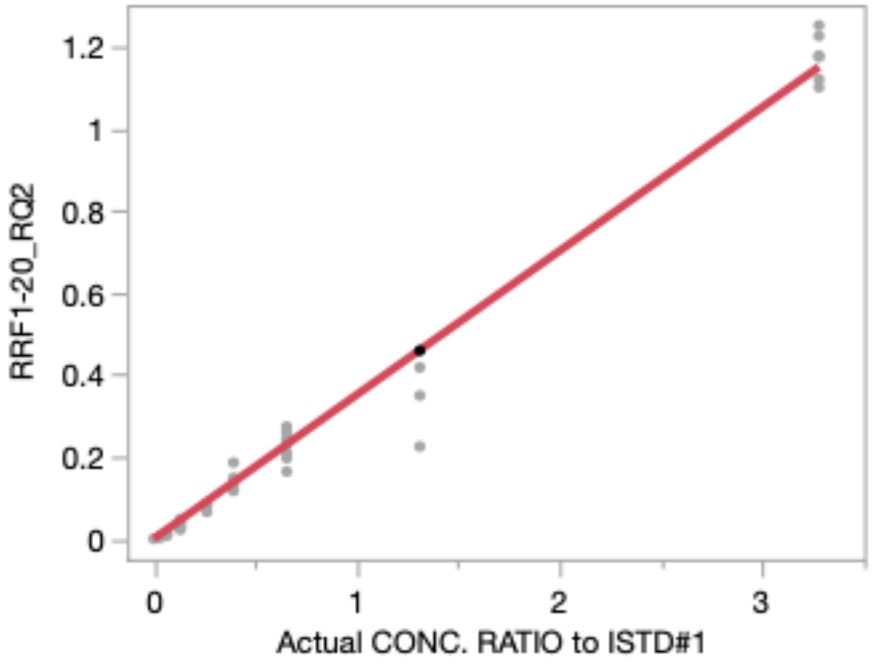

Figure C4. Calibration curve for C20:0 FAME, methyl arachidate.

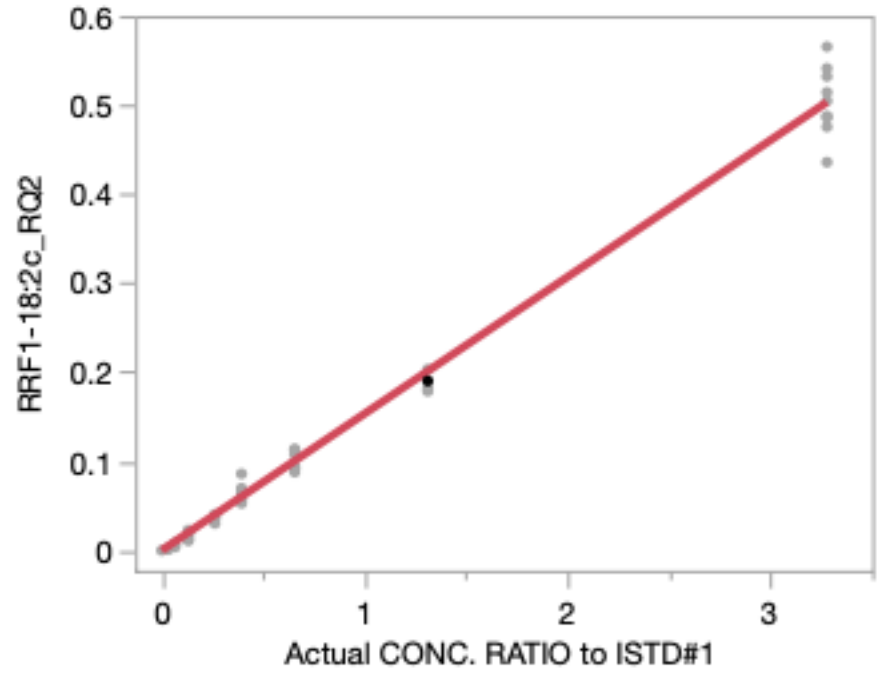

Figure C5. Calibration curve for C18:2cis FAME, methyl linoleate.

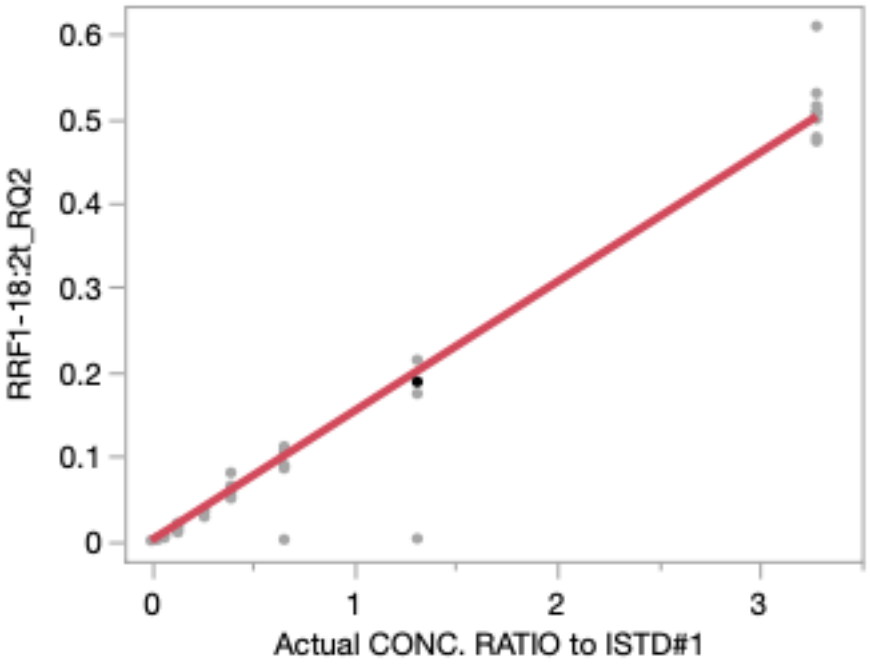

Figure C6. Calibration curve for C18:2trans FAME, methyl linoelaidate.

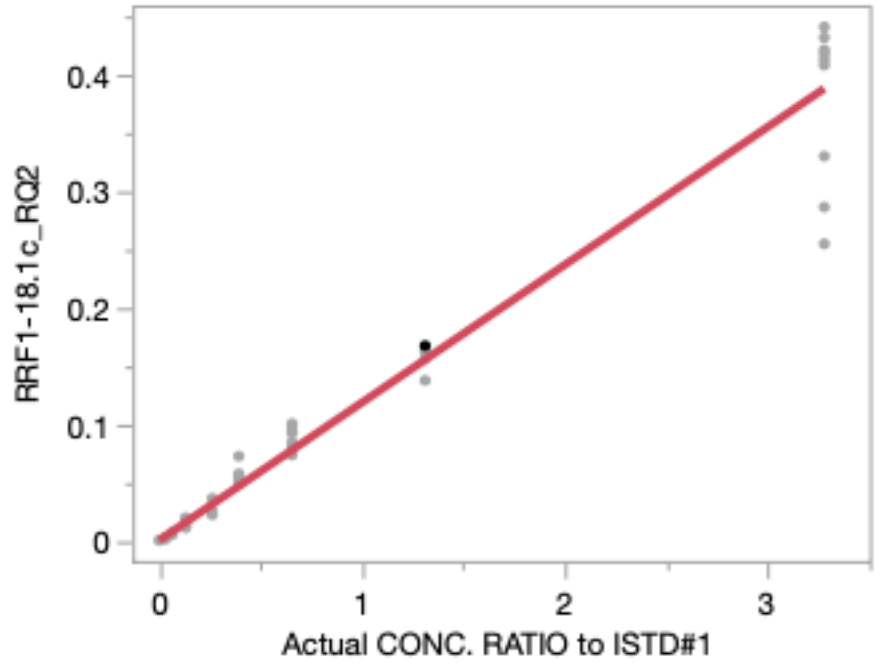

Figure C7. Calibration curve for C18:1cis FAME, methyl oleate.

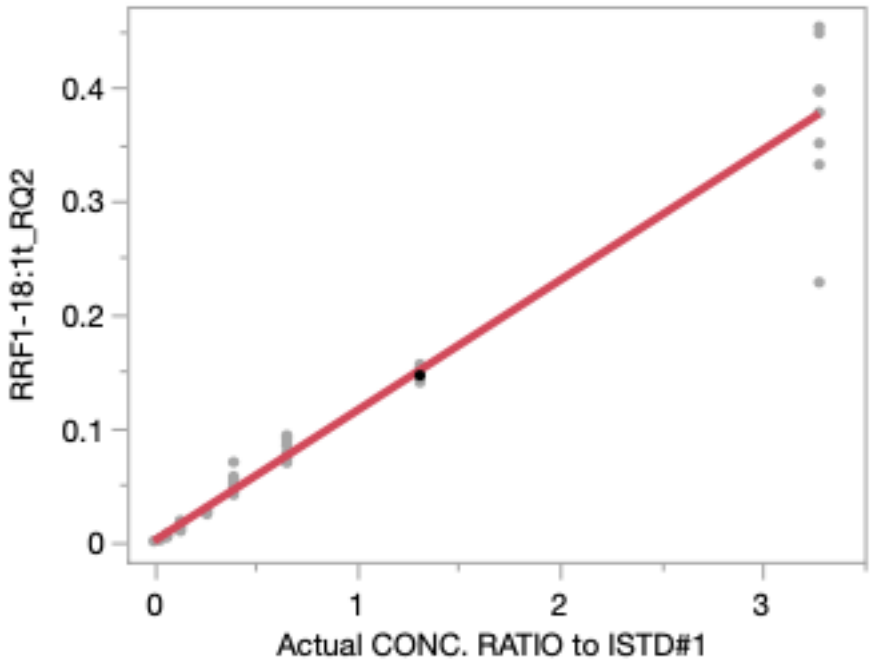

Figure C8. Calibration curve for C18:1trans FAME, methyl elaidate.

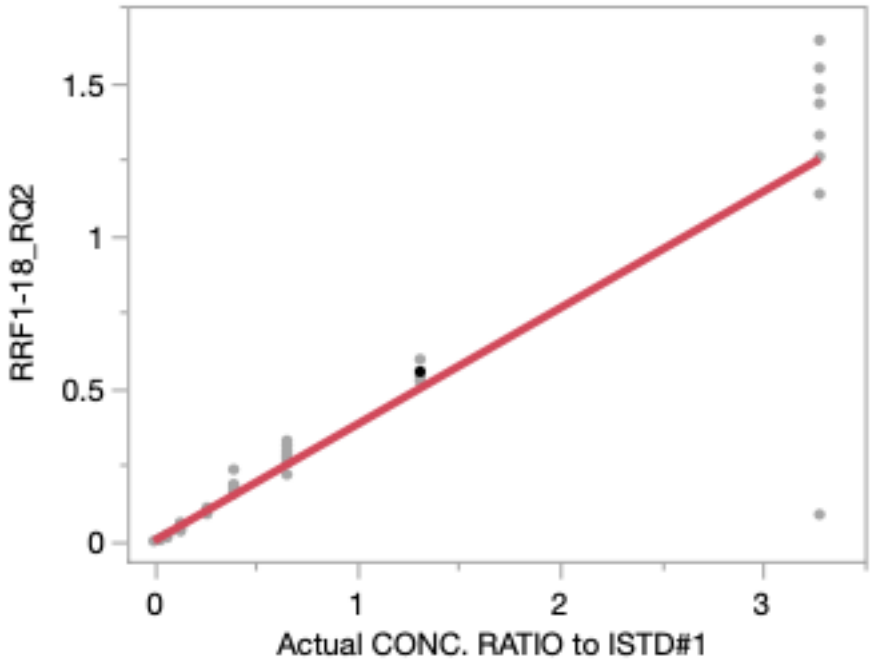

Figure C9. Calibration curve for C18:0 FAME, methyl stearate.

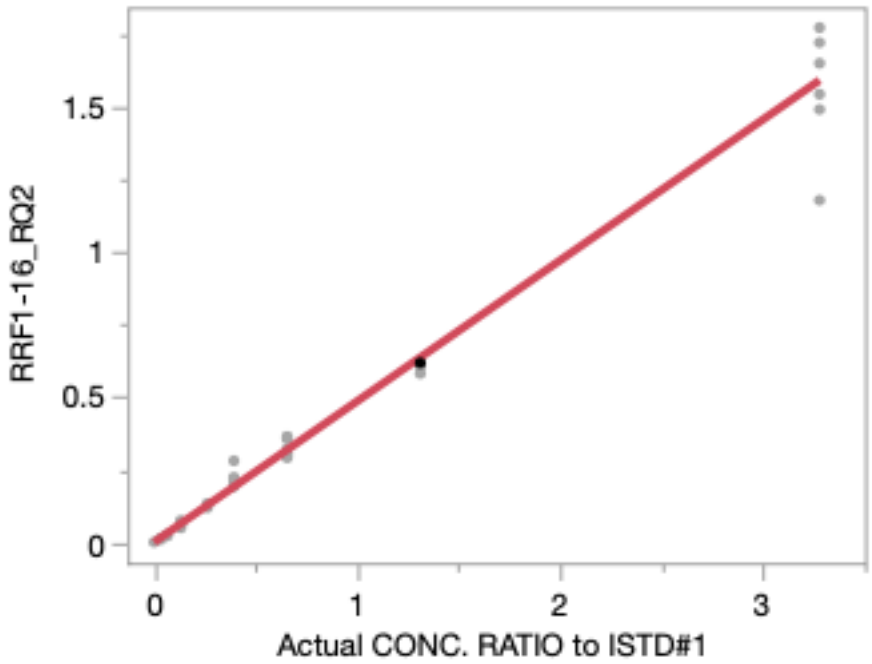

Figure C10. Calibration curve for C16:0 FAME, methyl palmitate.

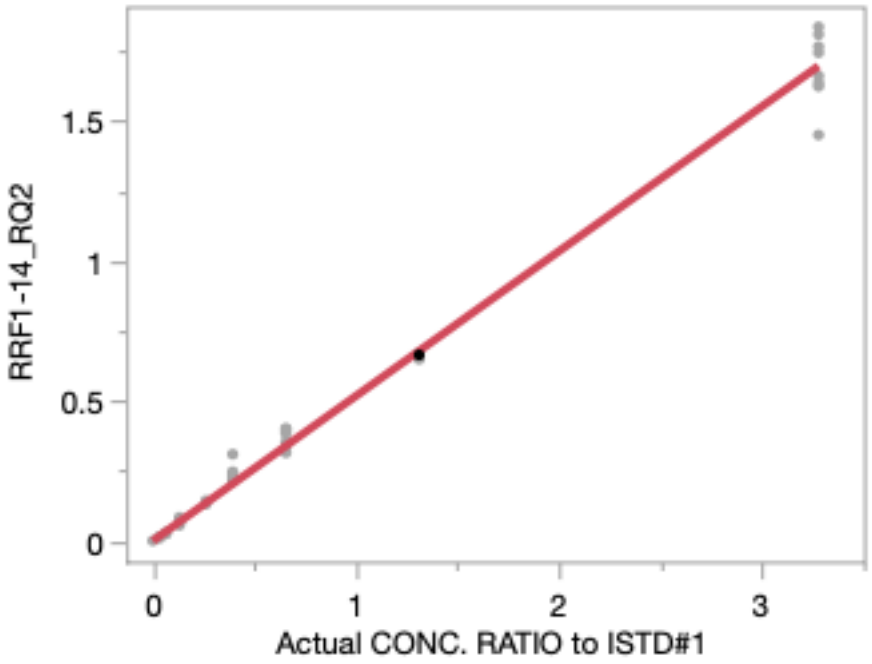

Figure C11. Calibration curve for C14:0 FAME, methyl myristate.

Table C3. GCMS calibration curve best-fit slopes for SIM Acquisition.

Chain	Common Name	Formal Name of Methyl Ester	MW	Cal Curve Slope
C14:0	Methyl Myristate	Tetradecanoic acid	228.38	0.5175
C16:0	Methyl Palmitate	Hexadecanoic acid	256.43	0.4863
C18:0	Methyl Stearate	Octadecanoic acid	284.48	0.3808
C18:1t	Methyl Elaidate	9E-Octadecenoic acid	296.48	0.1150
C18:1c	Methyl Oleate	Cis-9-Octadecenoic acid	282.47	0.1181
C18:2t	Methyl Linoelaidate	9E,12E-octadecadienoic acid	294.5	0.1532
C18:2c	Methyl Linoleate	Cis-9,12-Octadecadienoic acid	280.46	0.1536
C20:0	Methyl Arachidate	Eicosanoic acid	312.54	0.3515
C18:3n3	Methyl Linolenate	Cos-9,12,15-Octadecatrienoic acid	278.44	0.1726
C22:0	Methyl Behenate	Docosanoic acid	340.6	0.3147

Table C4. DTT activity (nmol DTT/min/mg PM).

Fuel Blend	Mean	SD	RSD %
B0	18.1	4.3	23.6
B20 NEAT	30.3	4.4	14.4
B20 OX2 (10 hr)	18.6	3.1	16.6
B20 OX1 (20 hr)	29.9	11.0	36.8
B100 NEAT	11.1	4.6	41.1
B100 OX3 (5 hr)	11.1	5.6	50.3
B100 OX1 (20 hr)	18.5	4.2	22.5

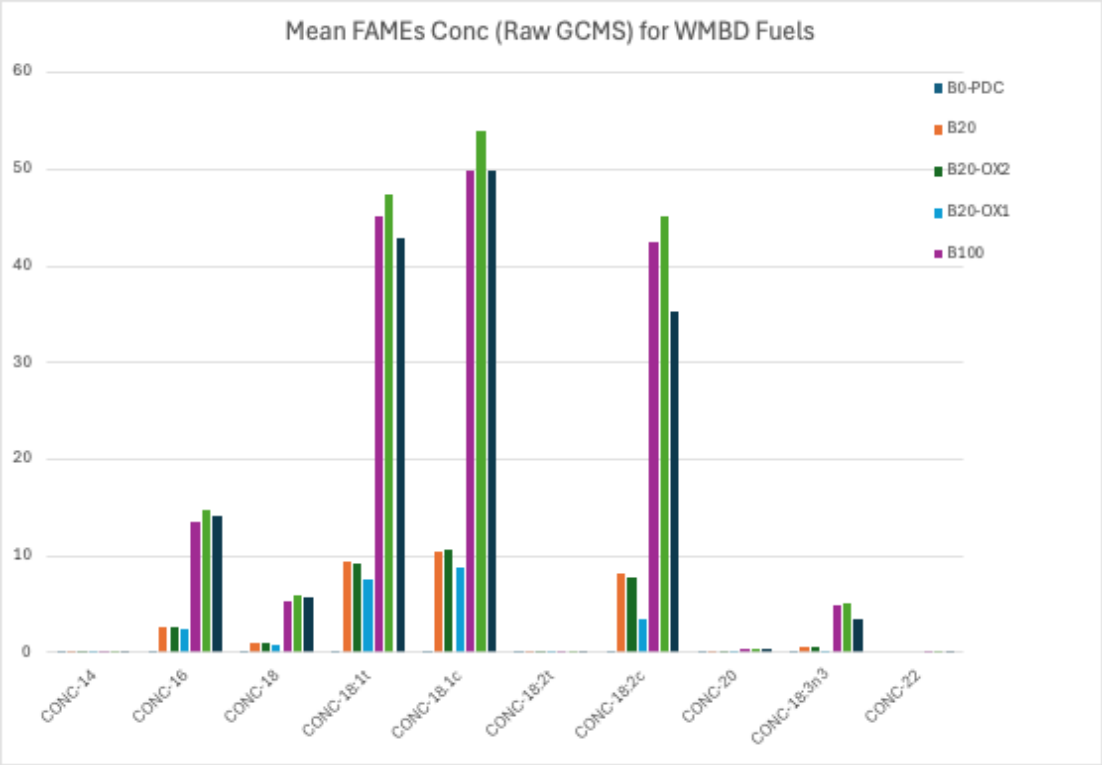

Figure C12. Mean concentrations (ng/uL) of individual FAMEs in B20 and B100 fuel.

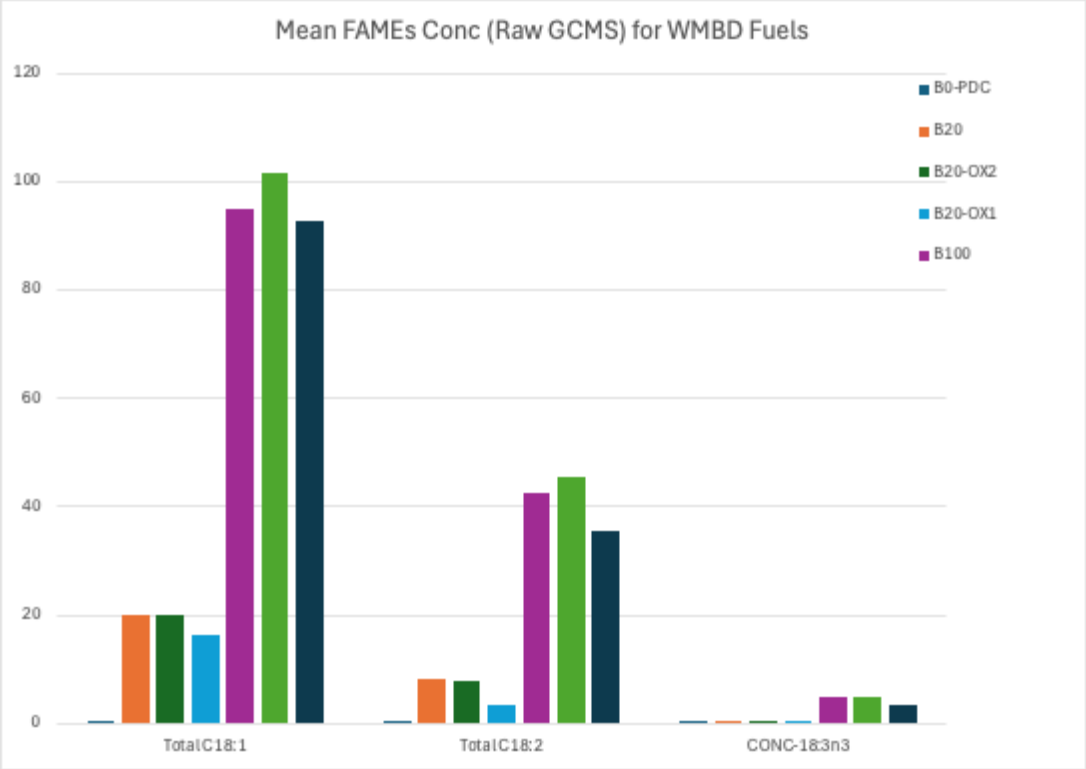

Figure C13. Unsaturated FAME concentrations (ng/uL) in B20 and B100 fuels.

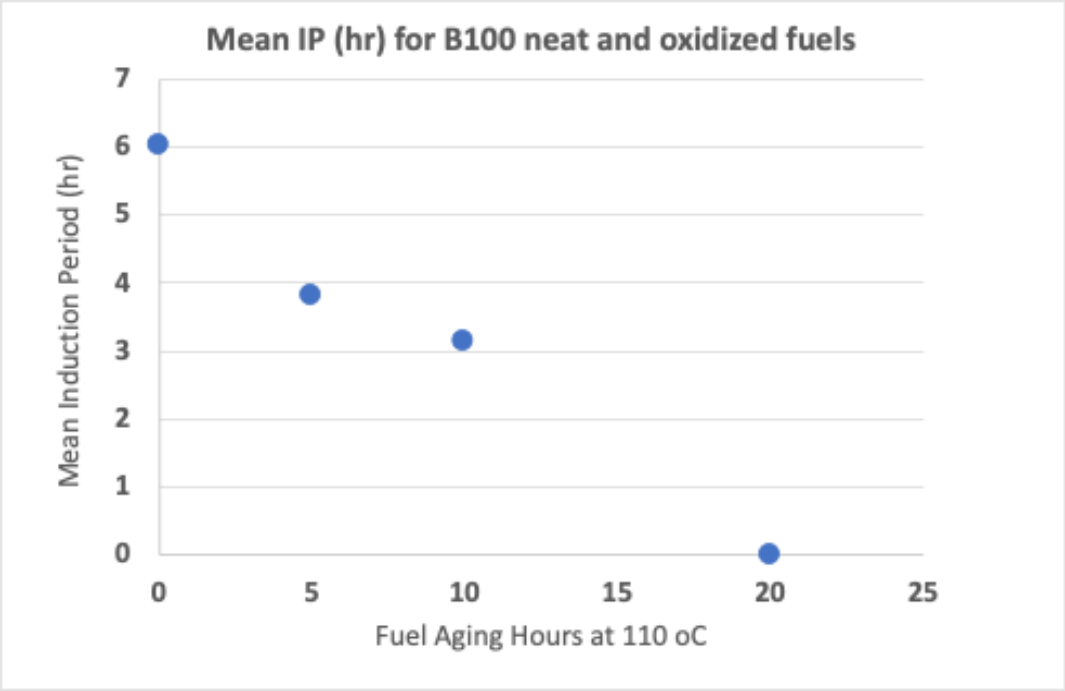

Figure C14. Induction Potentials measured by BOSS for WMBD B100 fuels of 0, 5, 10, 20 hrs of accelerated oxidation.